A Protocol to Measure Synaptosome Quantity in Rats Using Flow Cytometry

by

Wan Rong (Eunisse) Chua

A Thesis Presented in Partial Fulfillment
of the Requirements for the Degree
Master of Science

Approved October 2023 by the
Graduate Supervisory Committee:

Jonathan Lifshitz, Co-Chair
Timothy Balmer, Co-Chair
Ramon Velazquez

ARIZONA STATE UNIVERSITY

December 2023

ABSTRACT

Synaptosomes are isolated nerve terminals that contain pre- and post-synaptic proteins and can be used to model functionally intact synapses. While the quantification and characterization of synaptosomes have been used to study neurological conditions and diseases, relatively few studies have included the use of flow cytometry in the quantification and analytical processes. As such, this study highlights the use of flow cytometry in the synaptosomal quantification process and describes the adaptation of a previously performed synaptic flow protocol to find the optimal concentrations, protein-to-antibody ratios and gating strategies that meet the goals of this and future studies. To validate the protocol, three independent experiments measuring different treatments – traumatic brain injury (TBI), neurodevelopment, and ketamine - on synaptosomal quantity were conducted and compared to pre-existing literature. Despite the high standard deviation values between certain sample replicates, the synaptic flow protocol was validated by the right-skewed nature of the frequency distribution of the standard deviations between sample replicates and that most of the deviations fell below 40% of the maximum variance value. Further analysis showed significant differences ($p < 0.05$) between the ketamine and TBI groups compared to the control group while no significant differences were observed between the neurodevelopment (P30) group. This study validates the use of flow cytometry in synaptosomal quantification while providing insight to the potential of the synaptic flow protocol in future TBI and psychoplastogen studies.

ACKNOWLEDGMENTS

First and foremost, I would like to acknowledge my advisor, Dr. Jonathan Lifshitz, for being the most outstanding mentor. Along with the opportunity to pursue my passion for scientific research in his lab, I thank him for unwavering support and encouragement throughout my academic journey despite the numerous obstacles and challenges we faced. His dedication to research and education inspires me every day to continue pushing for my goals. If it were not for his exceptional guidance, kindness, and impeccable sense of humor, I would not be where I am today.

I would like to thank Dr. Timothy Balmer for sparking my initial interest in neuroscience along with the opportunity to explore this field. I also appreciate Dr. Ramon Velazquez for the helpful advice and valuable insights on neurodegenerative diseases and scientific research.

I would like to thank Luisa Rojas for her mentorship and patience throughout the research process, as well as for guiding me through the initial phases of my research. I am also very grateful to all members of the Neurotrauma and Social Impact lab for their endless support, thoughtful insights, and helping me grow personally and professionally.

Finally, I would like to give a shoutout to my family - my mother, father, sister, and partner, as they continue to cheer on while I reach for my dreams.

TABLE OF CONTENTS

Page

CHAPTER Page

LIST OF TABLES

LIST OF FIGURES

CHAPTER 1

OBJECTIVES & ORGANIZATION

1.1 Objectives & Goals

The objective of this thesis is twofold; first to adapt a previously performed protocol used to isolate and quantify synaptosomes in rat brains, and second to validate the adapted protocol by quantifying synaptosomes in rats subjected to three different manipulations. The utility of such a protocol enables a deeper understanding of neuronal systems by allowing more efficient comparison between the synaptosomes of rats subjected to various treatments, which serves as the ultimate goal of protocol adaptation.

1.2 Organization of Thesis

The thesis is divided into four chapters organized as follows: (1) an introduction to synaptosomes and the role in scientific discoveries; (2) adaptation procedures for the protocol and highlights of the challenges overcome to establish a final, working protocol; (3) application of the adapted protocol to investigate differences in synaptosomal quantity of rats subjected to different treatments; (4) a discussion of the study findings in relation to previous research, potential limitations, and implications for future studies to apply the protocol.

CHAPTER 2

INTRODUCTION

2.1 General Overview of Synapses and Synaptosomes

Even faced with modern technology, the exact function and role of many pieces and parts of the brain remain a mystery. However, significant advances in neuroscience have been made since the days of Ramon y Cajal's artistic depictions of neurons (DeFelipe & Jones, 1992). Through experimentation and observation using more advanced technology, neurons, the highly specialized basic units of communication in the brain, were discovered, followed by a detailed breakdown of the components that make them up. While the types and functions of neurons vary, they all share a cell body, axon initial segment, axon, and dendrites. Located at the interconnection between the axon and dendrite are synaptic terminals and spines, which together comprise synapses.

Synapses are gaps between two neurons, with one terminal termed the 'pre-synaptic' and the other 'post-synaptic'. The pre- and post-synaptic terminals of the synapse contain different proteins, receptors, and neurotransmitters specific to their function, and strategically localized to facilitate synaptic transmission between neurons (Letellier et al., 2019; Choquet & Triller; 2013). Synapses are generally classified into two distinct types: chemical and electrical synapses. While both types of synapses are used in neurotransmission, they differ in morphology, structure, and function.

Most synapses within the nervous system are chemical and will be the focus of this thesis. Chemical synapses usually contain larger gaps than electrical synapses, termed 'synaptic clefts', and communicate via chemical messengers, also known as neurotransmitters, in a complex chain of events (Südhof, 2013). Briefly, the

neurotransmitter-containing vesicles are synthesized and stored in the pre-synaptic terminal. As the action potential travels down the axon to depolarize the pre-synaptic terminal, the voltage-gated Ca^{2+} channels open and lead to an influx of Ca^{2+} to the terminal. This abundance of Ca^{2+} facilitates the binding of the neurotransmitter-filled vesicles with the pre-synaptic membrane and thus allows their contents to be released into the synaptic cleft, where the neurotransmitter molecules bind to specific ionotropic or metabotropic receptors on the post-synaptic terminal to exert their effects by changing the post-synaptic potential (PSP). These effects can be excitatory (EPSPs) or inhibitory (IPSPs), which increases and decreases the likelihood of an action potential being generated, respectively (Purves et. al, 2001). Whether a neurotransmitter exerts an EPSP or IPSP depends on the type of receptor that it binds to and the specific channels coupled to the receptor. In the nervous system, glutamate acts as the primary excitatory neurotransmitter when it binds to glutamate-specific receptors on glutamatergic neurons whereas gamma-aminobutyric acid (GABA) is the primary inhibitory neurotransmitter when it binds to GABA-receptors on GABA-ergic neurons (Allen et. al, 2023).

Electrical synapses, on the other hand, transmit signals more rapidly than chemical synapses but are less abundant throughout the nervous system (Bennett & Zukin, 2004). Electrical synapses contain specialized channels called ‘gap junctions’ which facilitate the speedy propagation of action potentials from the pre-synaptic to the post-synaptic terminal. The direct connection between the pre- and post-synaptic terminals allows for uninterrupted flow of current which allows for rapid neurotransmission. As ions flow from one terminal to another, the PSP is altered, leading

to EPSPs or IPSPs (Purves et. al, 2001). The differences in chemical and electrical synapses are summarized in **Figure 1** below.

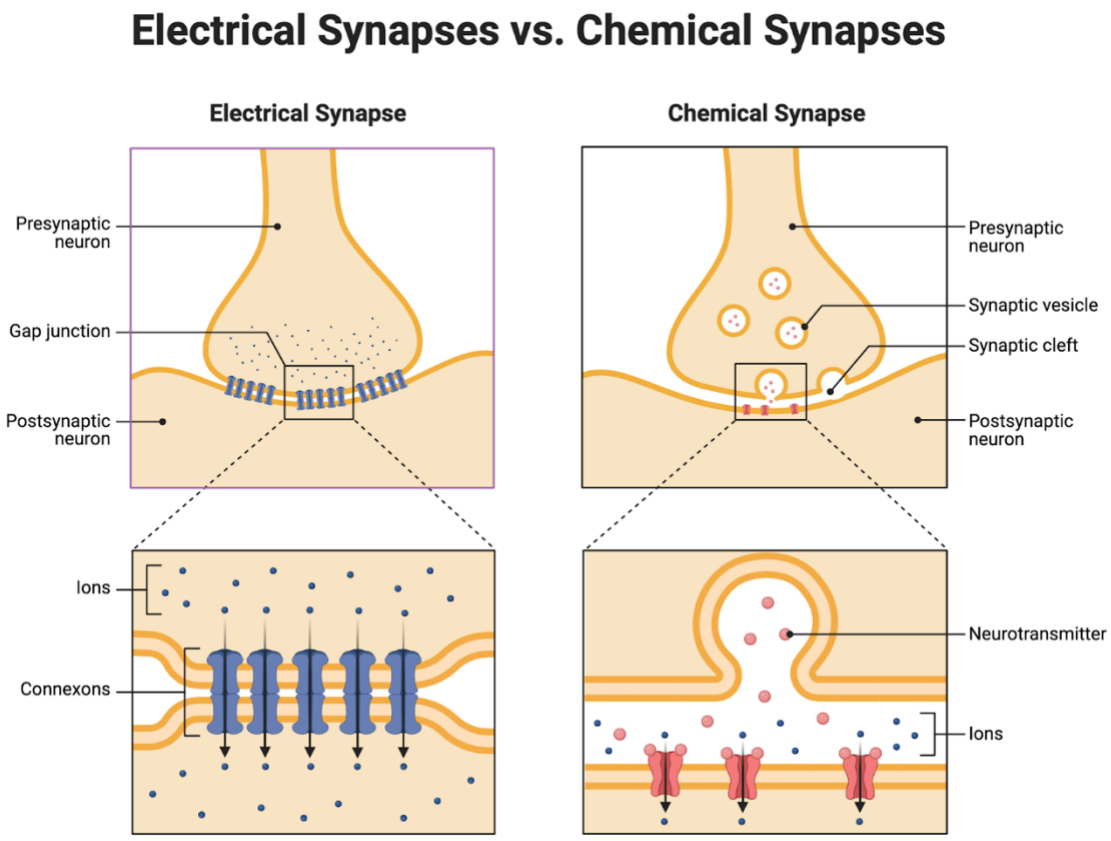

Figure 1 An overview of the morphological and functional distinctions between electrical and chemical synapses. Electrical synapses are connected via gap junctions while chemical synapses are connected via synaptic terminals and a cleft. Reprinted from "*Electrical Synapses vs. Chemical Synapses*", by BioRender.com (2023).

Techniques to identify the functions of synapses and neurotransmitters have seen significant advances to enhance our understanding of neurological diseases, along with the development of medication and treatment options (Hsia et al., 1999; Maksimovic et al., 2022). One such example is the drug Baclofen, originally developed to treat epilepsy,

muscle spasms and other spinal cord pathologies but is gaining popularity as treatments for a variety of clinical disorders such as musculoskeletal pain and gastrointestinal reflux disorder (Romito et. al, 2021). As an agonist for GABA-B receptors present throughout both the central and peripheral nervous systems, Baclofen works by binding to pre- and post-synaptic proteins to inhibit neurotransmission by slowing down the rate of action potentials and calcium signaling and thus relaxes muscles. Another example is Neostigmine, a drug that is often used to increase the rate of neurotransmission after a period of inhibition by anesthesia during surgical procedures (Neely et al., 2023). Neostigmine inhibits the enzyme acetylcholinesterase, which prevents the breakdown of the excitatory neurotransmitter acetylcholine (ACh) into its metabolites. This allows it to build up at the neuromuscular junction to a concentration where it can overcome the inhibitory effects of anesthesia, which restores muscle strength and contraction.

More recently, neurological injury and disease research has benefited from techniques to isolate and quantify synaptosomes. Synaptosomes are sealed, isolated nerve terminals from whole brains or brain regions that consist of pre- and post-synaptic proteins of synapses (Gray & Whittaker, 1962). Synapses consist of the pre-synaptic terminal and the post-synaptic dendritic spine in whole brain tissue whereas synaptosomes contain a lipid membrane alongside pre- and post-synaptic proteins and vesicles that have been pinched off and separated from the rest of the neuron through mechanical disruption and centrifugation, as shown in **Figure 2.**

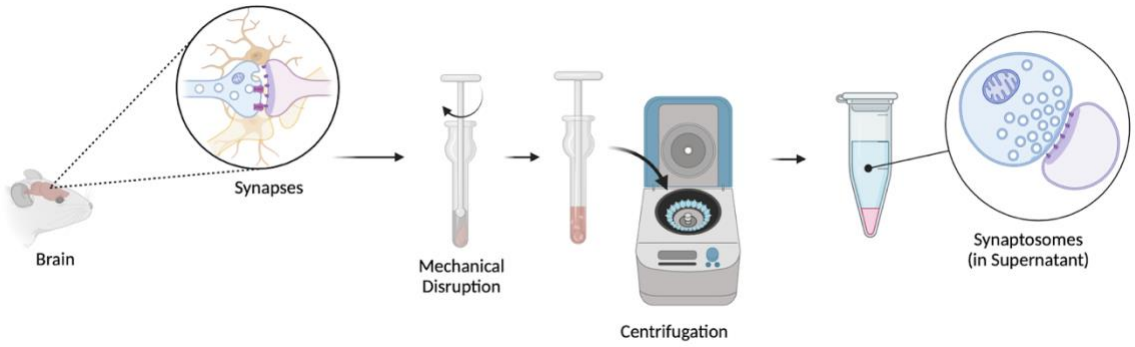

Figure 2 Distinction between synapses and synaptosomes, which are nerve terminals isolated through mechanical disruption and centrifugation. Created with BioRender.com.

2.2 Potential of Synaptosome Research

Since its discovery by Catherine Hebb and Victor P. Whittaker in the late 1950s (Hebb & Whittaker, 1958; Gray & Whittaker, 1962), synaptosomes have been used to better understand various neurological and metabolic processes. Compared to synapses, the isolated synaptosomes containing synaptic proteins and cellular machinery allows for more in-depth study of the mechanisms behind protein synthesis, membrane potential and ionic movements between neurons (Weiler, 2009). Synaptosomes also facilitated the initial identification of certain amino acids, such as glutamate, as neurotransmitters (Levy et. al, 1973; Sandoval et. al, 1978) while being a source of information of synaptic physiology to aid the investigation of regulatory signaling pathways (Evans, 2015) and how the release of these neurotransmitters is affected by neurotoxins such as α-latrotoxin, a compound found in the venom of the Black Widow spider (Terletskaya et. al, 1992). With the increased awareness of neuroinflammation in brain injury, more recent studies have seen synaptosomes to be useful in investigating the signaling processes and roles of specific proteins and cytokines in neuroinflammation (Trebesova & Grilli, 2023). A

recent study even found synaptosomes to be compatible vehicles for neuronal mitochondrial transplants to combat mitochondrial dysfunction that characterizes many neurodegenerative diseases (Picone et. al, 2021).

By first isolating synaptosomes and then identifying their contents, the types and roles of neurotransmitters involved in specific synaptic terminals and neurotransmission processes can be determined. This was shown by the results from Whittaker's (1959) synaptosomal studies investigating the location, mechanism, and function of the neurotransmitter acetylcholine (ACh) and its precursor, choline. Their findings regarding the intracellular distributions of ACh and choline within the vesicles contained in 'isolated nerve-endings', or synaptosomes, eventually illustrated the mechanisms of ACh release and its effects on the neuromuscular junction. This later led to the development of the first antibody to target cholinergic nerve terminals (Dowdall, 1975; Zimmermann, 2018). Further synaptosomal research by Whittaker also contributed to the current understanding of the physical and functional properties of synaptic vesicles alongside the characterization of proteins and lipids that they contain (Whittaker, 1962; Zimmermann, 2018).

Once isolated, synaptosomes can be prepared in different ways for analysis depending on the study goal or the properties investigated. To measure plasma membrane transporter activity and the endocytosis or exocytosis of synaptic vesicles, synaptosomes can be loaded with radioactive neurotransmitters such as GABA (Levy et. al, 1973). The mechanism of neurotransmitter release is illustrated via the detection of the movement of radioactively labeled GABA. This can also be done using high-performance liquid chromatography, enzyme-linked fluorometric assays or styryl dyes to measure

endogenous neurotransmitter release (Evans, 2015). Other techniques such as confocal microscopy, immunogold electron microscopy, western blots and proteomic analysis can be further be applied to synaptosomes for visualization, localization, and identification of synaptic proteins (Evans, 2015; Trebesova & Grilli, 2023). The application of these techniques allows synaptosomes to be used for investigating synaptic transmission and neuronal processes.

Today, the brain's capacity to change physically in response to various stimuli and experiences is known as 'synaptic plasticity'. This process describes the changes in neuronal processes and structures occurring on a micro-scale that form the basis of learning, memory, and adaptation (Ramirez & Arbuckle, 2016). The mechanism behind synaptic plasticity identified glutamate as the primary neurotransmitter involved in long-term potentiation (LTP), a mechanism heavily involved in Hebbian learning and memory formation (Purves et. al, 2001). LTP occurs when the ionotropic *N*-methyl-D-aspartate receptors (NMDARs) are activated by post-synaptic depolarization coinciding with released glutamate, although some more recent studies have shown that NMDARs themselves may be dynamically regulated and subjected to long-term synaptic plasticity (Hunt & Castillo, 2012). With isolated synaptosomes, the transmission of glutamate from the pre-synaptic terminal and NMDARs on the post-synaptic terminal may be tagged or labeled for further studies to facilitate the current understanding of the brain's role in learning, memory, and addiction.

By isolating the synaptosomes located in certain regions of the brain, comparisons can be made between the quantity and identity of neurons and proteins present, as illustrated by Paget-Blanc et. al (2022) where synaptosomes labeled with dopaminergic

markers were used to identify and characterize dopaminergic, glutamatergic, and GABA-ergic synapses as ‘dopamine hub synapses’ in mice striata. Given that synaptosomes maintain the molecular and biochemical properties of synapses, techniques can be further developed for application on animals or even in humans to investigate the pathology and mechanisms behind neurodevelopmental disorders, neurodegenerative diseases, or neurological conditions (Morini et al., 2021).

2.3 History of Synaptic Quantification and Analysis

2.3.1 Traditional Methods of Quantifying and Analyzing Synapses

Before the discovery of synaptosomes, the identification of synapses involved various staining and imaging methods. Staining methods include the Timms-sulfide silver protocol, which leverages the metallic properties of silver to form bonds with copper and zinc ions located in the pre-synaptic vesicles of synapses (Claiborne et al., 1989; Chicurel et. al, 1993). In synaptic terminals, the silver reagents react with the zinc ions, which are unusually abundant in nerve endings and thus can be used to characterize synapses and synaptosomal populations. After the tissue is fixed to preserve the integrity of neuronal structures, the silver-stained synaptosomes present in the brain sections can be visualized under an electron microscope.

Silver has also been used in procedures such as Golgi staining developed by Camillo Golgi back in 1873. It involves the impregnation of formalin-fixed, intact neurons and their cellular components - on sectioned slices of brain tissue - in a solution of potassium chromate and potassium dichromate (Baloyannis, 2015). This is followed by impregnation with silver nitrate solution, resulting in the formation of silver chromate deposits and giving neurons a deep dark or almost black-ish appearance against a yellow

background. Modifications to the protocol have been implemented throughout the years to increase reliability, with the Golgi-Cox staining method deemed as the most reliable in terms of staining axonal and dendritic arborization and spines through visualization of only a relatively low percentage of neurons (Zaqout & Kaindl, 2016). After development, the color change and contrast allow for microscopic visualization and quantification of evenly stained dendritic trees and spines, which are present consistently throughout the brain and serve as potential sites for synapse formation.

While not directly related to synaptosome quantification, counting individual synapses and synaptic clefts could estimate the number of synaptosomes within a brain region. Immunohistochemistry with antibodies specific to synaptic proteins can label synapses using a series of steps beginning with tissue fixation, paraffin-embedding, and sectioning (Henny et. al, 2010). The sections are then deparaffinized and rehydrated before antigen (or epitope) retrieval. Protein blocking is then implemented before incubating the tissue with primary and secondary antibodies. To facilitate the formation of insoluble, colored precipitates, chromogens that act as a 'detection system' such as 3,3-Diaminobenzidine (DAB) or NovaRed, are added. DAB is a substrate that binds to peroxidase enzymes conjugated to a primary or secondary antibody whereas NovaRed binds to alkaline phosphatase. After washing with Tris-buffered saline/Tween-20 solution and 5% dextrose, the tissue is counterstained with hematoxylin for increased contrast (Kim et. al, 2016; Magaki et. al, 2019). This enables the visualization of the neuronal components present in a brain section under light or even fluorescence microscopy if fluorescent compounds are used for labeling (Magaki et. al, 2019; Moreno et. al, 2022).

While the use of antibodies allows for specific targeting of different proteins on synapses or within neurons, IHC requires much time for completion and does not eliminate the need for manual labor when attempting to quantify the number of synapses in the brain. The results for IHC are also highly influenced by the thickness of the tissue, level of fixation and specific antibody labeling, which introduces potential areas for variability (Kim et al., 2016; Libard et al., 2018). With the quantity of synapses in a sectioned tissue found, the number would serve as a representation of the brain region. This extension of findings generalizes the number of synapses in one brain region by introducing potential inaccuracies that may arise from biological variation of each region alongside equipment limitations and pipetting errors. Most of the staining procedures are also done on tissue that has been previously fixed either in formalin or paraformaldehyde (PFA) which could have disrupted the biological processes or metabolic viability of proteins or neurons compared to using flash-frozen or fresh tissue samples (Dunkley & Robinson, 2018). These allow for the preservation of neuronal activity, ionic concentrations and structure as the enzymes and proteins in the brain are kept from denaturing due to a change in temperature or pH, whereas the cells are kept viable while being in a constant osmolarity.

2.3.2 Traditional Methods of Quantifying and Analyzing Synaptosomes

When synaptosomes were first discovered, they were thought to be structures analogous or similar to mitochondria where ACh was abundant (Hebb & Whittaker, 1958). Further investigation by Whittaker (1959) led to observations with electron microscopy where the ACh molecules were found to be located within synaptosomes, an entity distinct from mitochondria. In the early days of synaptosomal research, brain slices

were stained in osmium tetroxide and embedded in methyl methacrylate resin before the synaptosomes were isolated and visualized using electron microscopy to observe their contents, structure, and function (Whittaker, 1959; Gray & Whittaker, 1962).

With the increasing awareness that synaptosomes can be used to study a wide variety of neurological diseases ranging from traumatic brain injury (TBI) to Alzheimer's disease, strategies used to isolate synaptosomes from neurons have included the use of Teflon/glass tissue homogenizers and sucrose, Ficoll or Percoll gradients (Gylys et. al, 2000; DiGiovanni et. al, 2012; Booth & Clark, 1978). Upon homogenization of tissue from the region of interest, the mixture is centrifuged to separate the synaptosomes from the solution before being purified and placed on glass slides for visualization under an electron microscope.

With the development of modern technology, a commonly used technique in synaptosomal analysis is the application of western blots (Mahmood & Yang, 2012). Briefly, western blots allow for the identification and separation of specific proteins based on their molecular weight using gel electrophoresis and subsequent labeling with antibodies for protein visualization. In synaptosomal research, western blots are used to study the synthesis and misfolding of various synaptosomal proteins, the formation of protein complexes and can even facilitate the identification of biomarkers in neuroinflammation and autoimmune diseases (Trebesova & Grilli, 2023). This is demonstrated by Sokolow et. al (2012) where western blots were used to detect amyloid beta (Aβ) peptides and amyloid precursor protein (APP) in the synaptosomes of those affected with Alzheimer's disease. Recently, a similar approach was also used by Bruyère et. al (2020) to measure APP transport and regulation in subjects with Huntington

disease, where the levels of APP are observed to be regulated by the phosphorylation of the Huntingtin protein.

To quantify synaptosomal proteins, quantitative western blotting techniques have been implemented by measuring and comparing the intensity of a band of protein produced by SDS-PAGE analysis to the intensity of a band with a known concentration or quantity (Richter et. al, 2018). Once identified using techniques such as mass spectrometry, protein quantification methods include whole-cell stable isotope labeling, where the abundance ratios between the isotope-labeled proteins and the newly synthesized, unlabelled proteins, can be calculated using high-performance liquid chromatography (Oda et. al, 1999; Conrads et. al, 2001; McClatchy et. al, 2007). Other mass spectrometry approaches like intensity-based absolute quantification (iBAQ), comparative synaptosome imaging for semi-quantitative copy numbers (CosiQuant), and absolute quantification approach (AQUA) are used to estimate protein quantity by comparing the spectra of analyzed proteins or peptides to a standard either of an isotopically labeled peptide, varying immunofluorescence or protein intensities (Richter et. al, 2018).

Despite the use of these techniques in various studies to isolate and visualize synaptosomes, the challenge of quantifying synaptosomes in larger brain regions remains a challenge.

2.4 Flow Cytometry in Synaptosomal Quantification

Flow cytometry is commonly used to assess immune cell populations, such as red blood cells, platelets, and monocytes. The technique uses a combination of fluidics, optics, and electronics to measure cell sizes, shapes, and granularities as described by

McKinnon et al. (2018) and Hajjar et al. (2023) but is briefly described below. An outline of the major flow cytometry components and process are depicted in **Figure 3**.

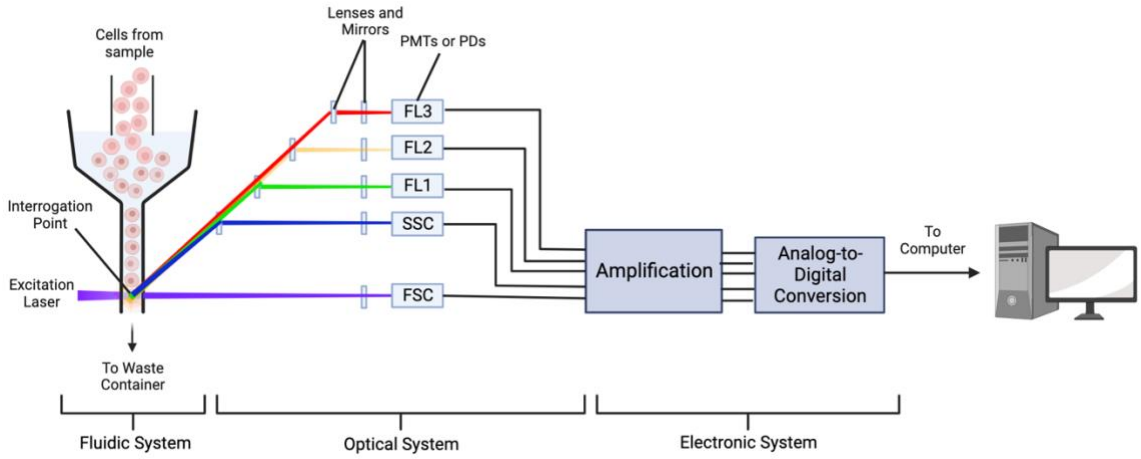

Figure 3 Outline of flow cytometry components and processes. Cells and synaptosomes are passed through the fluidic, optical, and then electronic components of the flow cytometer before being converted from voltage pulses to digital numbers for visualization and further analysis on computers.

The process begins at the fluidic system where cells, isolated synaptosomes with bound fluorophore-conjugated antibodies, or other unclumped biological components are suspended in sheath fluid. They are passed singly through an argon-ion laser beam (although more than one laser with different excitation wavelengths may also be used), arranged in a linear or parallel configuration. This process is known as 'hydrodynamic focusing' and occurs when the cross-sectional area of the flow cytometer's fluidics channel is altered to accommodate the flow rate of cells (Golden et. al, 2012). When the laser beam strikes a cell or synaptosome at the interrogation point, the subcellular components of cells or synaptosomes cause the laser to scatter and create unique diffraction patterns of forward (FSC) and side scattering (SSC). This can inform the size

and granularity of biological components passing through the laser and, when graphed, enables the identification of populations present in a sample, as shown in Figure **4**.

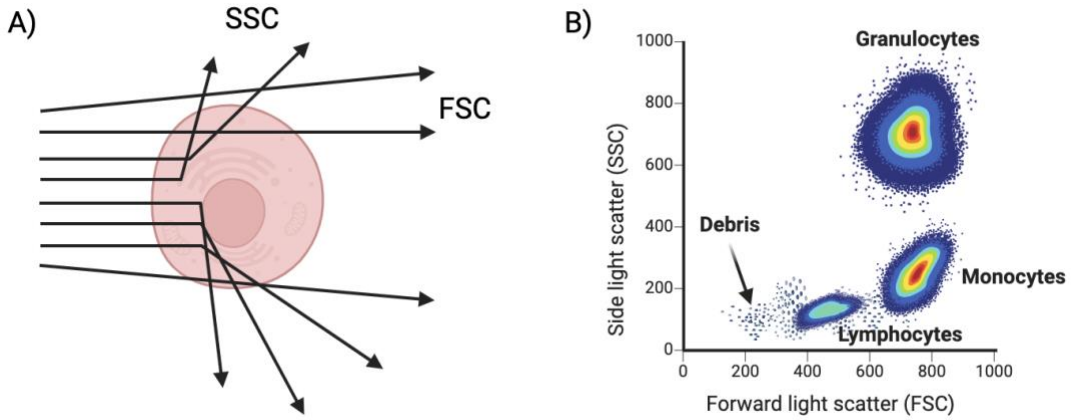

Figure 4 Flow cytometry mechanism to illustrate cellular characteristics. A) The scattering of the laser as it strikes the subcellular components (organelles, proteins) to create unique FSC and SSC patterns. B) The immune cells present in a sample are identified by the unique FSC and SSC values generated and grouped into populations on a graph. Each dot represents an event. The debris in a sample are usually identified by excluding events below certain FSC and SSC values.

Upon striking the cells, the energy in the monochromatic laser also leads to excitation of the electrons in the fluorophores attached to secondary antibodies (McKinnon et al., 2018). This is accompanied by subsequent emissions of specific wavelengths of light depending on the antibody profile. Now entering the optical system of the flow cytometer, these emitted light rays are split and filtered by dichroic mirrors, which are mirror-coated filters that allow only light of a certain wavelength to pass while the others are deflected or reflected in a specific direction (Steinkamp et al., 1974, Picot

et al., 2012). There are three general types of filters in flow cytometers: longpass, shortpass and bandpass. Longpass filters allow only light above a specific wavelength to pass through; Shortpass filters allow only light below a specific wavelength to pass through; Bandpass filters are a combination of short and longpass filters and allow a specific range of light to pass through.

After the light rays are filtered by wavelength, their signals are sent to detectors. These signals are electronically amplified when the photons emitted by the FSC, SSC or the fluorescence emission of fluorophores are detected by photomultiplier tubes (PMT) or photodiodes (PD) (Picot et al. 2012). Once the photons are in the detector, they are converted to electrons and the signal is multiplied proportionately. The resulting signal leaves the detector as a photocurrent and is amplified and converted into a voltage pulse, with the size of the pulse corresponding to particle size and fluorescence intensity. A voltage pulse can be characterized by its height or area. This pulse then undergoes analog-to-digital conversion (ADC) and becomes a digital number displayed on computers. Each signal generated by the emission of the laser scattering is registered as an ‘event’ and is used by the flow cytometer to plot the characteristics of populations and populations within a sample.

Since the range of sizes, shapes, and granularities of synaptosomes is distinct from other cells and debris, the light scattering produces a unique pattern to identify synaptosomes (El-Hajjar et al., 2023). When graphed, the forward scatter results inform about particle size and the side scatter illustrates particle complexity and granularity. Since synaptosomes are isolated nerve endings, they are smaller in size with less subcellular components, which correspond to lower FSC and SSC values compared to

cells. Once selected by physical features, antibodies to pre- and post-synaptic proteins, each with specific fluorophores, enables detection in the flow cytometer.

In this thesis, the protocol to discriminate and quantify synaptosomes from brain regions using flow cytometry will be referred to as ‘synaptic flow’. The protocol allows for the distinction and separation of synaptosome populations from cellular debris and other cells.

To isolate and quantify synaptosomes, the antibody incubation time is generally shorter for flow cytometry and avoids the use of highly toxic reagents. The synaptic flow protocol involves staining synaptosomes with two sets of primary antibodies each with their corresponding secondary antibodies, one set binding to the pre-synaptic terminal and post-synaptic terminal each. This allows synaptosomes to be ‘double-tagged’ and thus provide a clearer distinction between the synaptosomal population and debris or neuronal components that are not tagged with antibodies. The use of different sets of antibodies may increase precision when it comes to identifying synaptosomes and enables the different possibilities of pre-synaptic and post-synaptic proteins to be used in the process.

With the standardization of the sample protein concentration and number of events registered by the flow cytometer, flow cytometry reduces result variability from a variety of factors such as differences in sample preparation and human limitations. This limits the need for manual quantification while increasing the precision of double-tagged synaptosomes being measured in a short amount of time. It can also be used to study molecular alterations in post-mortem tissue of individuals with neurodegenerative

diseases, as done by Postupna et al. (2018) as a relatively fast and efficient way to characterize synaptosomes.

Compared to the lengthy processes of IHC, silver and Timms-sulfide staining of neurons which includes multiple steps and reagents that could affect the final staining and visualization of the results, fresh preparation of synaptosomes for flow cytometry allows the synaptosomes to be quantified in relatively intact conditions with minimal disruptions. This was demonstrated by Gylys et. al (2000) when the majority of synaptosomes stained using the viability dye Calcein AM throughout the sample preparation and flow cytometric process were found to be intact and viable. In a later study, this finding was further supported when Sokolow et. al. (2011) found that 99% of size-gated synaptosomes were labeled with Fluo-4NW, a calcium-sensitive dye indicating membrane intactness. With this, flow cytometry allows multiple parameters of individual synaptosomes, such as size, shape, and protein expression, to be measured simultaneously amidst samples with large numbers of synaptosomes.

The synaptic flow protocol was performed previously by Krukowski et. al (2021) when investigating the effects of deep space radiation on cognitive performance in rats. Amongst the different biomarkers used to assess the cognitive performance between rats subjected to a simulation of galactic cosmic radiation (GCRsim) and controls, rat hippocampal synaptosomes were quantified using flow cytometry as a means of assessing neuronal changes in relation to GCRsim-induced learning deficits. They found that rats subjected to 50 centigray (cGy) had significantly increased synaptosomal counts compared to control rats seven days after exposure. However, the rats exposed to 50 cGy of radiation and fed microglia-depleting (PLX5622) chow had hippocampal

synaptosomal counts similar to control rats. Combining these findings with other measured biomarkers, the researchers concluded that temporary microglia depletion shortly after exposure to GCRsim mitigated the synaptic changes and learning deficits induced by the simulation.

In conclusion, flow cytometry can be used to count large numbers of synaptosomes via the co-expression of protein-specific antibodies, which can increase the accuracy of synaptosomal identification. The synaptic flow protocol developed and published by Krukowski et. al (2021) serves as a useful resource that can be adapted to measure the effects of specific variables on synaptosomal quantity.

CHAPTER 3

SYNAPTIC FLOW PROTOCOL ADAPTATION

3.1 Overview of the Synaptic Flow Protocol

The synaptic flow protocol consists of four main components: synaptosome isolation consistent with the method depicted in **Figure 2** standardization of sample protein concentration; antibody staining; and flow cytometry, as previously done by Krukowski et. al (2021) and illustrated in **Figure 5**.

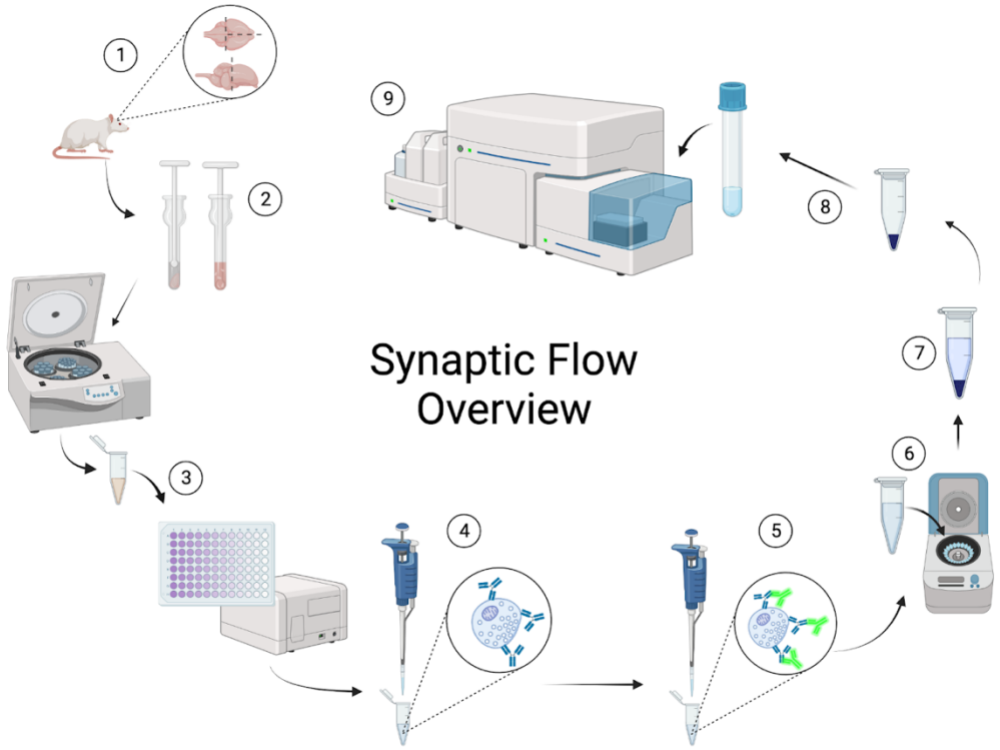

Figure 5 An overview of the synaptic flow protocol. Synaptosomes are isolated from brain tissue (1) using a 0.32 M sucrose gradient (2-3) and the protein concentration is standardized to 75 µg/mL (3). After Fc-blocking, primary (4) and secondary (5) antibodies are used to stain synaptosomes. After several rounds of washes (6-7), the

pellet of the solution is obtained (8) and fixed before flow cytometry (9). Created with BioRender.com

Synaptosome Isolation

From a fresh or snap-frozen brain, the region of interest was homogenized in 0.32 M sucrose with a 2 mL Teflon/glass Dounce homogenizer (DWK Life Sciences, Wertheim, Germany) for 10 times with a full clockwise turn of the homogenizer each time and centrifuged at 1200 x g for 10 minutes at 4 ℃ to isolate the supernatant from the pellet. The synaptosome-containing supernatant was then centrifuged at 13,000 x g for 20 minutes at 4 ℃ whereas the pellet consists mainly of unwanted tissues and was discarded. The pellet of this second centrifugation step contained synaptosomes and was subsequently diluted with 200 µL of phosphate-buffered saline for the determination of protein concentration.

Standardization of Protein Concentration

The protein concentration in the sample was standardized to 50 or 75 µg/mL using a BCA assay (Pierce™ BCA Protein Assay Kit, 23225, Thermo Fisher Scientific, Rockford, IL). The bicinchoninic acid (BCA) assay is amongst the most common techniques used to determine the protein concentration of a biological sample. Normalizing the protein concentration ensures that the stoichiometric ratio between protein and antibodies are appropriately matched during the subsequent labeling step. Proteins are measured by the reduction of Cu^{2+} ions to Cu^{+} ions in the presence of amino acids, most notably Tyr, Trp and Cys, including the peptide backbone present in biomolecules when subjected to basic conditions. This is known as the biuret reaction. BCA and the Cu^{+} ions produced in the biuret reaction react via a copper-chelation

mechanism. While a higher protein concentration in a sample does not necessarily correlate to a higher number of synaptosomes, standardizing the protein concentration across samples allows the equivalent amount of antibodies to be added for optimal labeling.

For each synaptic flow run, the protein in the homogenized samples were measured against a standard curve generated by increasing concentrations of bovine serum albumin (BSA). Upon incubation with BCA at 37 ℃ for 30 minutes, the well-plate containing the samples used to generate the standard curve and samples were put into a plate-reader to measure the optical density of each well. The optical densities of the wells containing BSA were then plotted against the increasing protein concentration to generate a standard curve with a linear equation that can be used to find the sample protein concentration using its optical density. From here, sample protein concentrations and sample volumes were standardized to 75 µg/mL and 200 µL, respectively, via the addition of phosphate-buffered saline (PBS). A worksheet was used to calculate the protein concentration and PBS to be added and is included in Appendix D of this thesis.

Sample Permeabilization

The synaptosomes were incubated in 100 µL of a fixation and permeabilization solution on ice for 20 minutes (0.1x BD Cytofix/Cytoperm™ Fixation/Permeabilization Kit, 554714, BD Biosciences, San Jose, CA) to permeabilize synaptosomal membranes and increase antibody staining of the synaptic proteins. This process also causes partial fixation of the samples to increase intracellular staining by antibodies.

Antibody Labeling

To reduce non-specific binding of antibodies, 0.2 µL of Fc-block (Human TruStain FcX™, 422301, BioLegend) inhibits the Fc-regions of non-synaptosomal populations. Fc-receptors are usually present in immune cells such as phagocytes and monocytes and specifically binds to antibodies to stimulate pathogen destruction (Mora & Rosales, 2009). Introducing proteins or antibodies that block Fc-receptors of non-synaptosomal populations minimizes non-specific synaptosomal staining as the synaptic flow results depend on the distinction between the negative and positive synaptosomal populations. As shown in **Figure 6**, Fc-block reduces the likelihood of false positive results. This step, despite not being part of the original protocol, reduced background signal during initial runs of the adapted protocol, as depicted by the more distinct clustering of events relative to the sample without Fc-block (see **Figure 7)**.

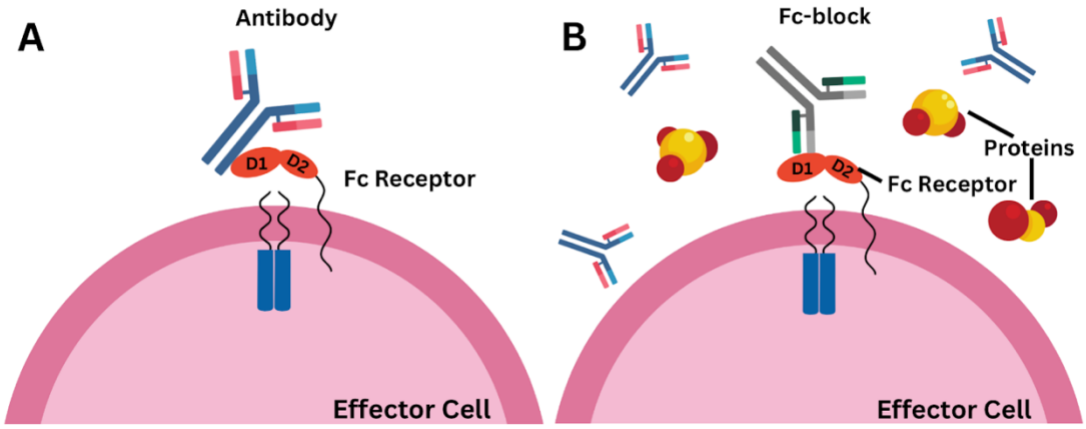

Figure 6 Fc-block mechanism of action. A) The binding of antibodies to the Fc-receptors of cells/membranes would increases the likelihood of non-specific labeling of non-synaptosomal elements. B) Addition of antibodies or proteins that specifically target and

bind Fc-receptors would ‘block’ the Fc-receptors, increasing the specificity of antibodies to stain synaptosomes.

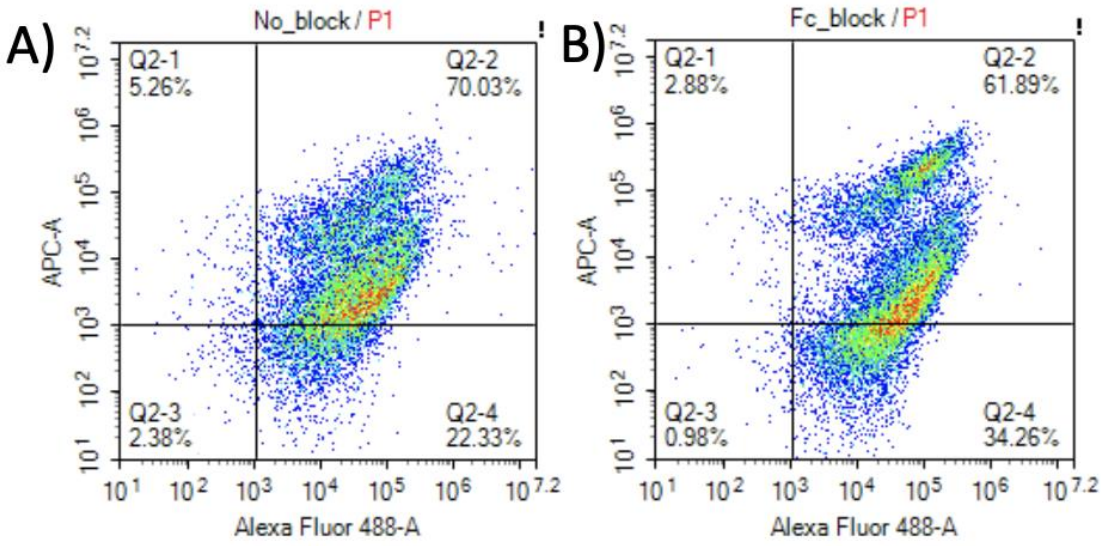

Figure 7 The dot plot of a sample stained with pre- and post-synaptic markers with Fc-block (B) has more distinct clusters of events than the sample without Fc-block (A).

Two sets of antibodies, each consisting of a primary and secondary antibody, were used to stain the pre- and post-synaptic terminal, although more antibodies may be added to stain specific components or proteins. In this study, rabbit anti-synapsin I and goat anti-rabbit APC were used as pre-synaptic markers; mouse anti-PSD-95 and goat anti-mouse Alexa Fluor 488 were used as post-synaptic markers, as summarized in **Table 1**. Synapsin I is a neuron-specific molecule with a key role in synaptogenesis and kinetic regulation of synaptic vesicle fusion (see **Figure 8**). While different neuronal subtypes contain different isoforms of Synapsin, the most common are isoforms Ia and Ib (Mirza & Zahid, 2018; Thiel, 1993). Synapsins facilitate synapse formation via the anchoring of synaptic vesicles to reduce neurotransmitter depletion at inhibitory synapses. By

organizing synaptic vesicles for exocytosis, Synapsin I also modulates neurotransmitter release. This was observed by Li et al. (1995) when the synaptosomes, electrophysiological responses, and synapses of Synapsin I-deficient mice revealed altered synaptic vesicle organization at pre-synaptic terminals, decreased neurotransmitter release, and delayed recovery of synaptic transmission after neurotransmitter depletion relative to wild-type mice. In the post-synaptic terminal, post-synaptic density 95 (PSD-95) is a member of the membrane-associated guanylate kinase family and regulates synaptic scaffolding in addition to synaptic plasticity. Overexpression of the PSD-95 protein blocked LTP and facilitated long-term depression (LTD) while decreased expression decreased LTD. Observation under a fluorescence resonance energy transfer (FRET) biosensor by Wu et al. (2017) showed that these processes are mediated by kinases and phosphatases that induce conformational switches and mutations at specific amino acids to increase the stability and interaction of PSD-95 to its binding partners. These targeted synaptic markers are retained in synaptosome preparations and depicted in **Figure 8**.

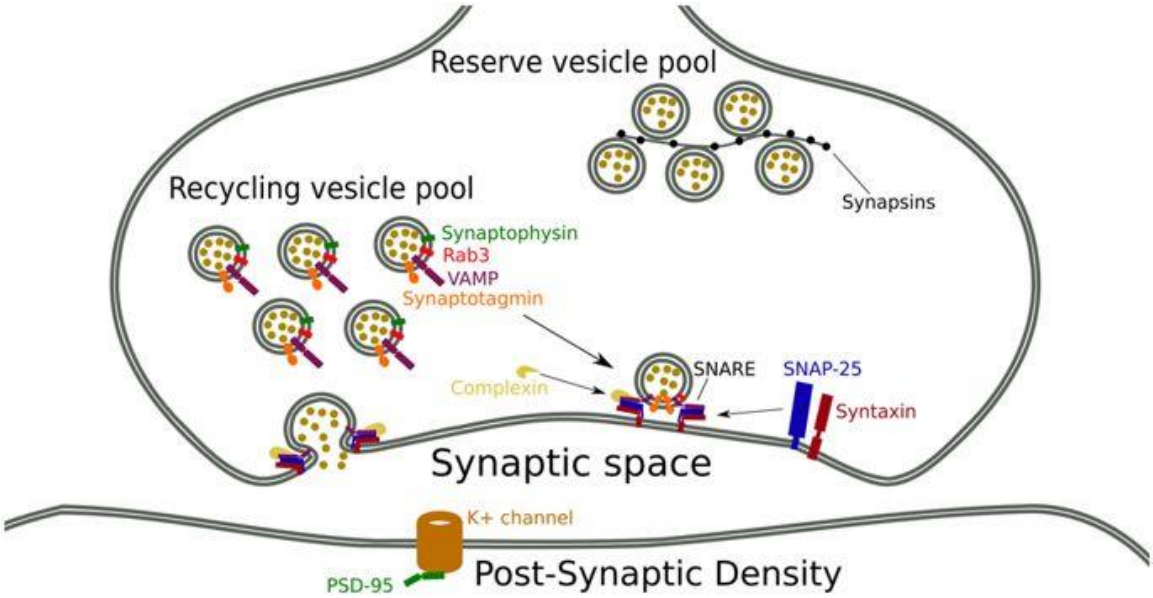

Figure 8 The Synapsins, consisting of Synapsin I and its isoforms Synapsin II and III, are proteins associated with vesicles located in the pre-synaptic terminal while the scaffolding protein PSD-95 is located at the surface of the post-synaptic terminal. Taken from Osimo et. al (2019).

Table 1

Primary and Secondary Antibodies for Labelling Pre- and Post-Synaptic Markers

	Pre-synaptic marker	**Post-synaptic marker**
Primary antibodies	Rabbit anti-synapsin I (Syn) (MAB1543, Millipore, Burlington, MA)	Goat anti-rabbit allophycocyanin (APC) (A10931, Invitrogen, Carlsbad, CA)
Secondary antibodies	Mouse anti-PSD-95 (PSD-95) (ab13552, Abcam Cambridge, UK)	Goat anti-mouse IgG (H+L), Cross-Adsorbed Secondary Antibody, Alexa Fluor™ 488 (A11001, Invitrogen, Carlsbad, CA)

Note. The table above shows the pairs of primary and secondary antibodies used to label the pre-synaptic and post-synaptic elements as components of isolated synaptosomes for flow cytometry.

The synaptosomes were incubated in primary antibodies at a concentration of 0.005 µg/µL for 30 mins at room temperature and agitated after 15 minutes to promote binding opportunities. To wash the synaptosomes, 750 µL of Perm/Wash Buffer (554723, BD Biosciences, Franklin Lakes, NJ) was added before centrifugation at 13,000 x g for 5 minutes at 4 ℃ and the supernatant was discarded. The staining process was then repeated with the secondary antibodies (0.01 µg/µL for 488 and 0.0025 µg/µL for APC) incubated at 4℃ in the dark. The wash step was then repeated for a total of three times after antibody incubation.

Tissue Fixation

Prior to flow cytometric analysis, the samples were fixed with 200 µL of 2% PFA stored at 4 ℃. To maintain the quality of the fixation process, fresh batches of 100 mL 2% PFA were prepared each week via the addition of 2 drops of 1M sodium hydroxide (NaOH) and 2 g paraformaldehyde prills (Fisher Scientific, 50-276-34) in 100 mL of 60 ℃ PBS.

Flow Cytometer Setup

The NovoCyte Quanteon Flow Cytometer (Agilent Technologies, Santa Clara, CA) was used to collect synaptosome counts among 30,000 events for each sample. A quality control (QC) test was performed daily using freshly prepared QC beads (1 drop of beads with 500 µL of PBS or 400 µL of PBS and 100 µL of 1X NovoRinse). After ensuring that the QC test passed, a new experiment was created and ‘Auto

Compensation' settings were used to establish compensation controls. The compensation, described in detail in a later section, was run based on the parameters of area vs area and the appropriate detector voltages were set for each fluorophore: 300 V for FSC, 265 V for SSC, 515 V Alexa-Fluor 488 and 675 V for APC. After collecting 10,000 events for compensation, the FSC vs SSC and positive/negative gates are automatically adjusted but may be altered by clicking on the gate, deleted or adjusted using the keyboard and arrow keys. When this process was completed for all three sets of compensation beads, the compensation matrix was applied to the experiment by clicking and dragging Compensation to the untitled.ncf and selecting 'New Specimen'. This can also be achieved by making a new Specimen and Sample by right clicking and selecting 'Rename'.

To set up the parameters for sample event collection, the sheath fluid flow rate was set to 10 µL/min and the stop condition was set at 30,000 events, and the threshold of exclusion was set to 50,000 on FSC-H. The option to rinse the sample-collection probe was also selected to ensure minimal carry over between samples. Prior to placing the sample in the tube holder for data collection, 200 µL of freshly prepared flow cytometry-assisted cell sorting (FACS) buffer was added into each tube and vortexed to mix with the fixed synaptosomes. A total of 30,000 events were collected for each sample and visualized using dot plots. Gating strategies are described in a later section and were completed by selecting the icons corresponding to each type of gate. A detailed protocol of this process is attached in **Appendix A** of this thesis.

Compensation

In flow cytometry, compensation involves the digital removal of any fluorochrome from all detectors except the one devoted to measuring the signals from a specific fluorochrome. This is crucial in preventing the spillover between fluorescence signals as the flow cytometer is able to detect the fluorescence emitted by each distinct fluorochrome on beads or cells and calculate the amount of fluorescent signal spillover of each fluorochrome into the detection channel of another fluorochrome. The unwanted fluorescence signal can then be subtracted from the other detection channel to correct for the spectral overlap and thus allowing accurate fluorescence values for each fluorochrome used in the experiment to be obtained.

Gating for the synaptosome populations was completed using 1, 3 and 6 µm beads, which corresponded approximately to the synaptosomal diameter of 0.5 to 1.5 µm (Picone et al., 2021; Gulyássy et al., 2020). The compensation controls were completed using either synaptosomes or UltraComp EBeads Compensation Beads (01-2222-41, Thermo Fisher Scientific, Waltham, MA) that were incubated with either a set of pre- or post-synaptic antibodies and washed alongside experimental samples for a total of 4 times with 750 µL of Perm/Wash Buffer. Since the centrifugation of beads at 13,000 x g for 5 minutes at 4 °C does not generate a visible pellet, 50 µL of the solution was left in the tube after each wash and the supernatant was discarded. Each drop of compensation beads contains spherical particles of two populations: a positive one that will capture any mouse, rat or hamster antibody and a negative one that is unreactive to antibodies. An ‘unstained’ set of beads is one containing only one population - beads or cells without antibodies added. For each experiment, there was an approximate 50-50 split between the

positive and negatively stained population of the beads incubated with the pair of pre-synaptic or post-synaptic antibodies relative to the unstained beads. This maintains compensation quality as the separation of the two populations detects the presence and intensity of a fluorescence signal and serves as a means of calibrating the instrument to ensure reproducible experiments. An example of the distinction between the positive and negative population for the pre- and post-synaptic markers is depicted in **Figure 9**. A total of 10,000 events each were obtained for the three sets of beads.

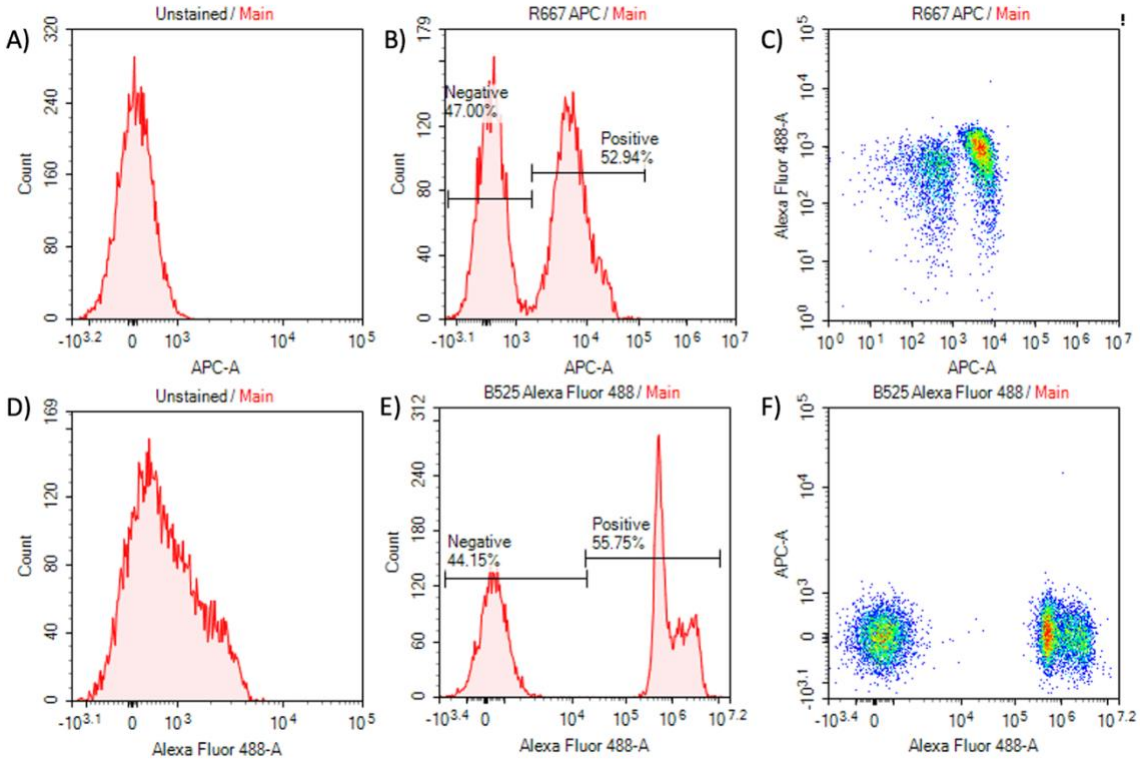

Figure 9 A) The population of the unstained beads measured in the APC channel. B) The approximately 50-50 split between the populations of beads incubated with the pre-synaptic antibodies Synapsin I and APC. C) A dot plot of the split populations of Synapsin I and APC. D) The approximately 50-50 split between the population of the unstained beads measured in the Alexa Fluor 488 channel. E) The split populations of

beads incubated with the post-synaptic antibodies PSD-95 and Alexa Fluor 488. F) A dot plot of the split populations of PSD-95 and Alexa Fluor 488.

3.2 Applications for Data Analysis

The applications NovoExpress (Agilent Technologies Inc.) and FlowJo (v10, TreeStar Inc.) were used to analyze the count data.

The initial graphs of SSC vs FSC were plotted using a linear scale and a polygon gate was drawn to select the 'center' portion of the data while leaving out the 'front' and 'tail'. From this population, a graph of APC (Synapsin 1) vs Alexa Fluor 488 (PSD-95) was plotted on a logarithmic scale. Here, a 'population' refers to the events measured within a quadrant or gate. The negative control, a sample containing synaptosomes but no antibodies, was used to establish the boundaries of the quadrant gates where the population is split into four quadrants. All quadrants other than the bottom left were kept below 1% in conjunction with the quadrant boundaries kept between 10^3 and 10^4 events, as depicted in Section A of **Figure 10**.

Gating for the synaptosome populations was completed using 1, 3 and 6 µm beads as well as using guidelines set by Krukowski et. al (2021). Briefly, from the linear scale graph of SSC vs FSC, the center portion of the 'comet-shaped' population was gated to select the 'P1' population, avoiding the area of the densest signals (red) and the tail of comet, as shown in **Figure 11**. The P1 population represents the events that are within the size range of synaptosomes.

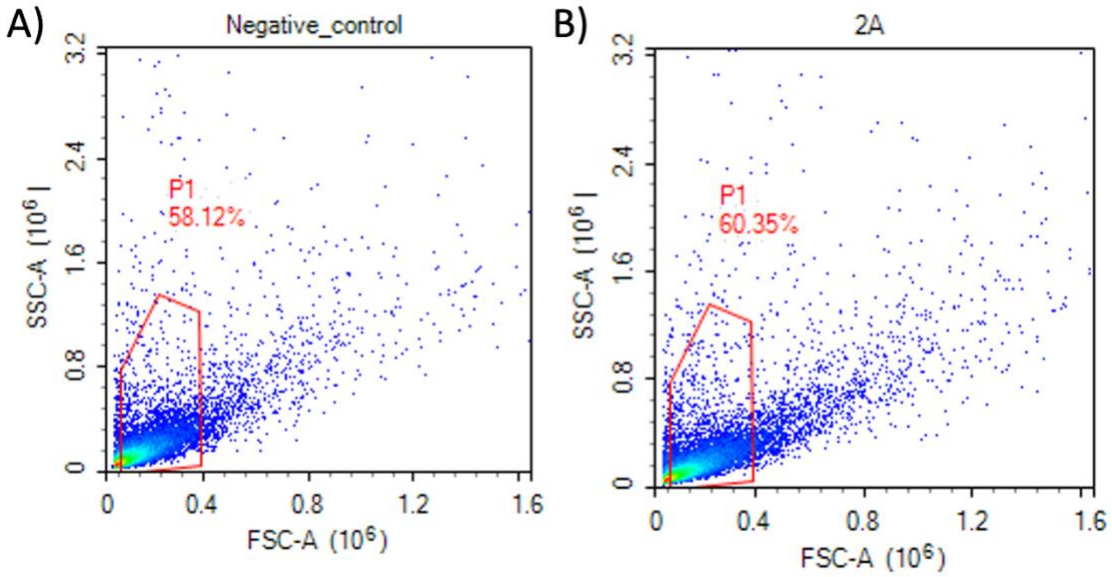

Figure 10 Gate used to select the P1 population of the 'comet'-like plot of the (A) unstained synaptosomes and (B) synaptosomes stained with pre- and post-synaptic antibodies on the linear graphs of SSC-A (area) vs FSC-A.

Gating Strategies

After gating by size to identify the P1 population, different gating methods were tried to identify an approach to isolate the target synaptosome population, as shown in **Figure 11**. The gating methods included a 'quadrant' gate that split the plot into four quadrants on the logarithmic graph depicting the fluorescence intensity of APC vs Alexa Fluor 488, based on the negative control for each experiment. The gates were added so that the majority of the negative population was contained in the Q3 quadrant, while the Q1, Q2 and Q4 quadrants had <1% of fluorescence intensity. The population in Q1 and Q4 represents the events that express only the pre- or post-synaptic markers, respectively; Q2 represents the events that co-express both pre- and post-synaptic markers; Q3 represents the events that do not express any markers. From here, the percentage of

events in Q2 alone and Q2+Q4 were obtained, with the addition of Q4 being due to an issue observed with the pre-synaptic markers discussed in detail in a later section. Other gating methods such as the ‘negative-naught’ and the ‘floating population’ gate were also trialed. The negative-naught gate was drawn based on selecting the events outside of the negative control, ensuring that the gate included only the events above 10^3 on the APC-A scale and 10^4 on the Alexa Fluor 488 scale with less than 1% of events when applied to the control. This population represents the events that occur outside of those present in the negative control. The floating population gate was drawn based on a sample with a second cluster of events present, ensuring that most of the events within that cluster are included in the gate for comparison to samples with only one cluster of events. This population represents a second cluster of events which may be a more specific type of synaptosomes. The gating strategy chosen for further comparison in the synaptic flow protocol validation experiments will be explained in a later section.

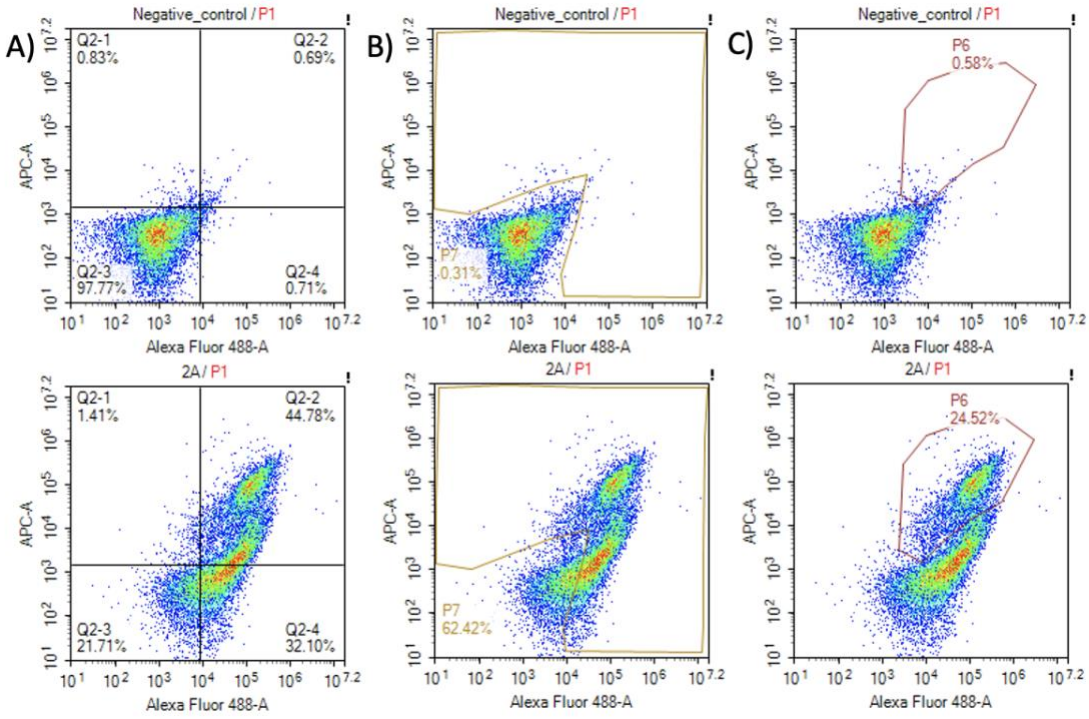

Figure 11 The gating strategies that were trialed in the protocol adaptation process. A) The 'quadrant' gate was drawn based on the negative control to ensure that all quadrants other than Q3 (Q2-3) had <1% of fluorescence signals. B) The gate was drawn based on the negative control so that the majority of the population other than the negative control was included in the region. This is termed the 'negative-naught' population and is represented by P6. C) Due to the presence of a second cluster of events, this gate was drawn based on the 'positive control' which is a sample that showed a significant population relative to the negative control. This is termed the 'floating' population and is represented by P7.

3.3 Protocol Adaptation: Challenges, Results and Improvements

A series of trials focused on replicating the protocol set by Krukowski et. al (2021) and formed the basis of the working synaptic flow protocol described in **Sections**

3.1 and **3.2**. This section recounts the challenges and obstacles experienced and overcome, where the synaptic flow protocol was adapted to meet the experimental goals of this thesis.

The ideal concentration of the sucrose gradient was confirmed to be isotonic at 0.32 M by the observation that a higher number of synaptosomes were isolated when compared to a lower concentration of 0.16 M. The isotonic sucrose is consistent with the original isolation protocol developed by Gray & Whittaker (1962).

Minimal to no pellet was collected during a wash step after standardizing the protein concentration to 50 µg/mL. Exceptionally high fluorescence intensity signals were observed with the incorrect protein-antibody ratio. To confirm an ideal protein concentration that results in a visible pellet and a suitable protein-to-antibody ratio for staining, titrations were conducted for both protein and antibody concentrations. Protein concentrations of 50, 75, 100, 250 and 500 µg/mL and both primary and secondary antibody concentrations of 0.5x, 1x, 2x and 3x relative to their original concentrations were subjected to the synaptic flow protocol. The concentration of 75 µg/mL and original (1x) antibody ratios produced a consistent pellet and increased difference in synaptosomal counts between stained samples and controls.

Early variations of the protocols resulted in non-specific staining as observed by unusually high fluorescence intensities in samples stained with only a pair of pre- or post-synaptic markers relative to the negative control. FBS and an Fc-block were trialed to minimize non-specific antibody staining of non-synaptosomal populations. The Fc-block showed an increased defined distinction between stained samples and controls and thus was adapted as part of the protocol.

In data collection, the compensation and PMT voltage settings of the flow cytometer had influenced the resultant plots. Various voltage settings and compensation methods were tested using both compensation beads and synaptosomes. The established voltages were 300 V for FSC, 265 V for SSC, 515 V Alexa-Fluor 488 and 675 V for APC, which aligned with a protocol by Hobson & Sims (2019). It was also found that incubation of compensation beads with both primary and secondary antibodies alongside the synaptosomes produced a distinct separation of positive and negatively-stained populations for optimal compensation. Therefore, flow cytometry compensation for each run was completed using three sets of polystyrene beads: one with no antibodies, one stained with the pre-synaptic markers and one stained with the post-synaptic markers.

CHAPTER 4

CHARACTERIZATION OF SYNAPTOSOME QUANTITY IN RATS

4.1 General Experimental Approach

To validate the adapted synaptic flow protocol, three independent experiments were conducted using rat brain to measure synaptosome quantity in response to (i) TBI; (ii) neurodevelopmental stages of synaptic pruning, and (iii) administration of high dose ketamine.

Once harvested, fresh brain tissue samples were used in the synaptic flow protocol detailed in **Section 3.1**. Briefly, the tissue was homogenized, and its protein concentration was standardized before antibody staining and quantification in the flow cytometer. Four gating strategies were applied to analyze synaptosome populations, in accordance with the aforementioned methods, namely Q2 or Q2+Q4 populations of the quadrant gate, the negative-naught population, and the floating population.

For all experiments, rat cortical hemispheres were processed for synaptic flow, which aids in the analysis and comparison of experimental findings. Changes in synaptosomal counts and profile in the cortex have also been observed when rats were subjected to TBI, synaptic pruning, and ketamine administration. By referring to previous findings regarding the changes in synaptic and synaptosomal quantity in response to these treatments, the adapted synaptic flow protocol can be validated.

4.2 Synaptosomes in Three Experimental Conditions

First, an experimental model of TBI highlights the potential importance of synaptosomes in neuropathological studies. Second, emphasis is placed on the role of synaptosomes in measuring synaptic growth and the effects of neurodevelopment. Finally, the delivery of

the psychoplastogen ketamine is employed to highlight changes in synaptosome quantity in developing psychiatric and neurological interventions.

4.2.1 The Effect of TBI on Synaptosomal Quantity in Rats

Introduction to TBI

With increasing reports regarding head injuries in athletes, veterans and victims of violence or abuse, TBI is a growing public health concern and the leading cause of mortality after other physical traumas. Over 50 million TBIs occur around the world annually, both in underdeveloped and highly developed countries alike (Maas et. al, 2017; DeCuypere et. al, 2012). It occurs when the impact of an external force on the brain causes the deformation of brain tissue, altered brain function, or neuropathology. TBI can be caused by a combination of biomechanical conditions including, but not limited to: rotational forces, accelerating/decelerating forces, blunt impact, penetration from a projectile, or blast-wave exposure (McKee & Daneshvar, 2015; Giordano & Lifshitz, 2021). Depending on the magnitude of mechanical force, location of trauma, genetic factors, and pre-injury lifestyle, the resultant pathophysiology and clinical symptoms are used to classify TBI severity into categories such as mild, moderate, debilitating, and fatal (Giordano & Lifshitz, 2021). However, given the variability of symptoms even amongst patients with similar injury designations, the complex interaction between pathophysiology, biological sex, age, and physical activity levels post-injury can make it difficult to distinguish between the patients who recover and those with chronic morbidities (Iverson et al., 2017; D'Lauro et al., 2018; Leddy et al., 2019; Willer et al., 2019). Some of the most common enduring symptoms are broadly classified as cognitive, somatic, or emotional, although most TBIs usually resolve

between 1 to 10 days post-injury (DPI) and more long-term negative outcomes are usually associated with increasing injury severity (Giordano & Lifshitz, 2021).

While there are other qualitative types of TBI, the focus here is placed on diffuse TBIs, the most common form presented in clinical settings. Diffuse TBIs are induced by inertial forces exceeding a specific threshold. The tissue shear and distortion at the time of injury lead to axonal, hypoxic-ischemic, and microvascular injuries (Giordano & Lifshitz, 2021). Diffuse TBI also damages vascularization, leading to synaptic loss, behavioral deficits and morbidity as damaged circuits undergo reorganization in an attempt to restore homeostasis (Lifshitz et al., 2016; McKee & Daneshvar, 2015). In a laboratory setting, diffuse injuries can be modeled via the midline fluid percussion injury model (mFPI) that represent mild and diffuse clinical brain injury due to the acute and late-onset behavioral deficits and morbidities (Rowe et al., 2016). Primary injuries are irreversible and refer to direct damages resulting from impact such as blunt-force trauma, penetrating injuries and rapid acceleration and deceleration of the head. Contrarily, secondary injuries encompass the neuropathology that results from primary injuries, which may be reversible. These injuries may present as ischemic and hypoxic damage, increased intracranial pressure, or cerebral edema from the initiation of complex inflammatory signals on a cellular level.

On a pathological level, TBI has been shown to disrupt neurological function with pathophysiology that differs by TBI mode and severity. The acute neuropathological effects of TBI range from ionic and metabolic disruptions in neurons, diffuse axonal injury, vascular disruption and dysfunction, inflammation, to alterations in neural circuitry (McKee & Daneshvar, 2015). On the other hand, more chronic pathophysiology

present in TBI survivors may be associated with the onset of neurodegenerative diseases such as dementia, Alzheimer's, or Parkinson's disease (Moretti et al., 2012; Graham et al., 2023; Amerongen et al., 2022). Recent studies have emphasized the implications of TBI-induced diffuse axonal injuries on microtubule function, leading to synaptic loss and increased amyloid-beta plaques and neurofibrillary tangles (Tagge et al., 2018; Graham & Sharp, 2019; Mac Donald et al., 2007).

With its varying clinical presentations and post-traumatic conditions, the importance of understanding the neuropathology associated with TBI at different time points (acute, subacute, chronic) post-injury cannot be overstated. Knowing how TBI impacts neuronal growth, death, and neurotransmission can facilitate the comprehension of disease progression in a temporal manner. Based on a previous study by Giordano et al. (2022) where the neuropathology of TBI rats at 1, 7, and 28 DPI was compared, the neuropathology across all brain regions increased acutely from 1 DPI to subacute time points around 7 DPI. Other studies on mice and humans have also demonstrated an accumulation of TBI-induced neuropathology. Observation under diffusion tensor imaging showed decreased white matter fractional anisotropy whereas observation under electron microscopy showed decreased synaptic connectivity and neuronal proliferation from acute to subacute time points in those subjected to TBI compared to controls (Edlow et al., 2016; Singh et al., 2006).

Despite the increasing availability of treatments for TBI such as surgery, therapy and medications, patients often suffer from permanent brain damage or disabilities (Lifshitz et al., 2016). The pathophysiology that results from different types and severity of TBI at different time points post-injury can serve as biomarkers in the diagnosis and

prognosis of TBI. This is demonstrated by the clinical translation of experimental studies such as the timing of decompressive craniectomy in the alleviation of intracranial pressure (Zweckberger et al., 2006). Zweckberger et al. (2006) found that early craniectomy reduces brain edema and secondary brain damage using mice that were subjected to TBI and decompressive craniectomy at time points ranging from 2 hours to 7 DPI. Experimental studies measuring the effects of hyperbaric oxygen therapy and Ca^{2+}-channel blockers on injury pathophysiology have also informed the behavioral outcomes of TBI and intensive care unit monitoring on blood pressure, glucose and oxygen metabolism, and cerebral blood flow (Xu et al, 2010; Maeda et al., 2005).

Goals and Hypotheses

Although TBI biomarkers and pathophysiology have been researched, few have investigated the effects of TBI on synaptosomal quantity.

TBI neuropathology includes synaptic loss, axonal damages and mitochondrial dysfunction. As a homeostatic response, inflammatory molecules, such as cytokines and reactive oxygen species, are activated and thus alter signaling cascades and synaptic quantities (Giordano & Lifshitz, 2021). Synaptosomes are isolated synaptic terminals containing pre- and post-synaptic proteins that can be used in the detection of changes in synaptic numbers (Trebesova & Grilli, 2023) given that many of the neuronal metabolic and enzymatic activities are preserved in synaptosomes (Ahmad & Liu, 2020). As such, it was hypothesized that the cortices of rats subjected to TBI induced using a mFPI model would have lower synaptosomal counts compared to uninjured sham rats 7 days post-injury.

Animals

Adult male Sprague-Dawley rats (n = 12, 6-7 weeks; Harlan, IN) were acclimated to the university vivarium for 7 days after arrival. The animals were housed in cages of 4, in a 12 h light: 12 h dark cycle at a constant temperature (23 ℃), with food and water available *ad libitum* according to the Association for Assessment and Accreditation of Laboratory Animal Care International. The rats were 8-9 weeks postnatal at the time of tissue collection, with the timeline of events illustrated in **Figure 12**.

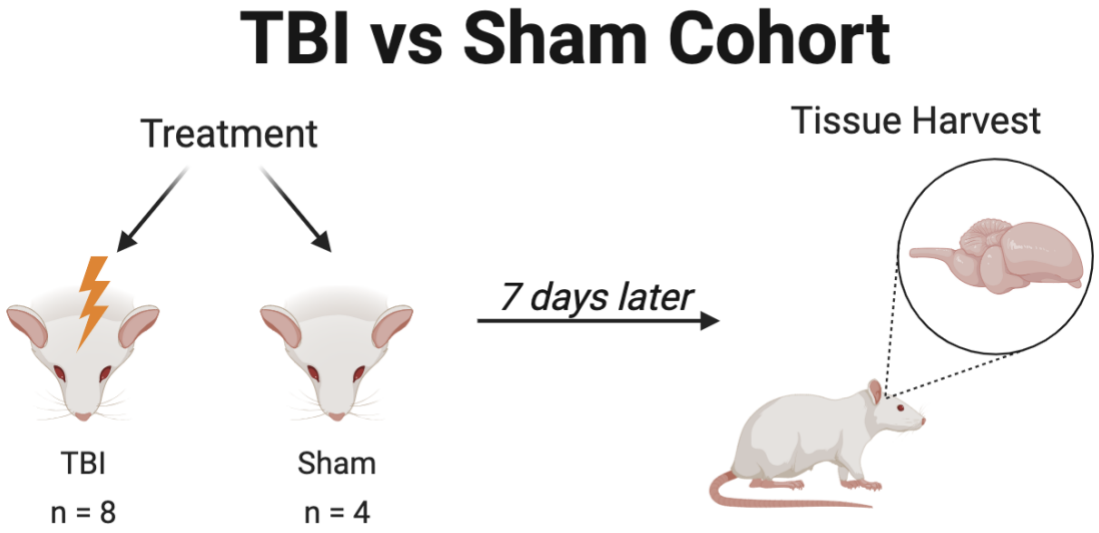

Figure 12 The timeline of events for the rats in the TBI vs sham experimental cohort. Rats were acclimated for 7 days and separated into two groups for injury. Post-operative monitoring was conducted from 1 to 3 DPI and the brain tissues were collected at 7 DPI. Created with BioRender.com.

Midline Fluid Percussion Injury (mFPI)

Rats were subjected to midline fluid percussion injury (mFPI) consistent with the methods described by Giordano et. al (2022), which are included here. At the time of

surgery, rats were anesthetized using 5% isoflurane in 100% oxygen for 5 minutes and the head of the rat was placed in a stereotaxic frame with continuously delivered isoflurane at 2.5% via a nose cone. During surgery, body temperature was maintained at 37°C with an isothermal heating pad (Braintree Scientific). A midline incision was made exposing bregma and lambda landmarks on the skull. Fascia was removed from the surface of the skull. A trephine (4.8 mm outer diameter) was used for the craniectomy, centered on the sagittal suture between bregma and lambda without disruption of the dura. A skull screw was secured in a 1-mm hand-drilled hole into the right frontal bone. An injury cap prepared from the female portion of a Luer-Loc needle hub was fixed over the craniectomy using cyanoacrylate gel and methyl-methacrylate (Hygenic Corp, Akron, OH). The incision was sutured at the anterior and posterior edges and topical Lidocaine ointment was applied. Rats were placed in a heated recovery cage and monitored until ambulatory.

For injury induction, rats were re-anesthetized (60-90 min after surgery) with 5% isoflurane delivered for 5 minutes. The dura was visually inspected through the hub to make sure it was intact with no debris. The hub was then filled with normal saline and attached to the male end of the fluid percussion device (Custom Design and Fabrication, Virginia Commonwealth University, Richmond, VA). A diffuse brain injury (1.8-2.0 atm) was administered by releasing the pendulum onto the fluid-filled cylinder. Sham-injured rats underwent the same surgical procedures except the pendulum was not released. Rats were monitored for the presence of a forearm fencing response, and righting reflex times were recorded for the injured rats as indicators of injury severity. The righting reflex time is the total time from the initial impact until the rat

spontaneously rights itself from a supine position. The fencing response is a tonic posturing characterized by extension or flexion of the forearms that has been validated as an overt indicator of injury severity. The injury hub was removed, and the brain was inspected for uniform herniation and integrity of the dura. The dura was intact in all rats and none were excluded. The incision was cleaned using saline and closed using staples. Diffuse brain-injured rats had righting reflex recovery times between 6 to 10 minutes and a positive fencing response. Sham-injured rats recovered a righting reflex within 20 seconds. After spontaneously righting, rats were placed in a heated recovery cage and monitored until ambulatory (approximately 5-15 minutes) before being returned to their cage.

Adequate measures were taken to minimize pain or discomfort throughout the process and the rats were monitored for post-surgical complications for 3 days after injury. A total of 2 animals experienced complications from technical issues during surgery and were euthanized during injury.

4.2.2 The Effect of Synaptic Pruning in Development on Synaptosomal Quantity in Rats

Introduction to Synaptic Pruning

Specialized equipment has discovered the changes that occur in neurodevelopment. Amongst these discoveries are the vast changes in neuronal and synaptic quantity throughout the neurodevelopmental process.

During the early stages of neurodevelopment, synapses are overproduced and later ‘pruned’ away to form neural circuits, where unnecessary synapses are eliminated (Navlakha et al., 2015; Sakai, 2020). In humans, synaptic density increases from the

earliest embryonic stages, peaking around 2 years of age before it declines by 50-60% upon reaching adulthood. This targeted elimination of functional synapses is the process known as ‘synaptic pruning’ and results in the strengthening of synapses in relevant neural circuits. This allows increased efficiency of neurotransmission between the strengthened circuits, while other synaptic connections weaken and fade (Navlakha et al., 2015). The factors that determine which neuronal circuits are strengthened are multifold, including high frequency of use and constant sensory, motor, and cognitive input that reinforce the synaptic connections. In contrast, the connections that are inadequately stimulated are pruned (Santos & Noggle, 2011). The influence of neural activity on the developmental rewiring of the brain was initially made by Hubel and Wiesel (1963) in their study where cats were monocularly-deprived during their developmental period. Strengthened synaptic connections in the visual cortex of the open eye and weakened connections for the sensory-deprived eye were observed, suggesting a link between neural activity and plasticity. Since then, similar studies have been conducted on various species such as monkeys and ferrets to further support this relationship between neural activity and plasticity (Hubel et al., 1977; Yu et al., 2011). As a key mechanism used to regulate neuroplasticity, synaptic pruning functions to shape individual learning and memory-formation processes in response to experience.

Synaptic pruning is predominant in the early years of life through adolescence and is orchestrated by specific proteins and cellular signaling cascades. In a developing brain, the sculpting of synaptic connections is influenced by the specific neural pattern of activity and time of activation, guided by individual experiences (Faust et al., 2021). Given the interplay between synaptic pruning and neuroplasticity in the formation of

neural circuits, a determinant of these processes is the activation frequency of NMDARs, similar to the mechanisms of synaptic plasticity described in **Section 1.4**. The synaptic connections with weak activation levels get flagged for destruction by microglia, which become phagocytic in the brain (Paolicelli et al., 2011; Morini et al., 2021). The interaction between microglia and developing synapses can also be mediated by the complement cascade as part of the innate immune system. In this mechanism, C1q, the protein that initiates the classical complement cascade and complement receptor 3 (C3), a downstream protein, tag CNS synapses for elimination by microglia (Schafer et. al, 2012; Stephan et al., 2012). By sorting and analyzing synaptosomes tagged with Anti-C1q antibodies, Györffy et al. (2018) discovered a link between apoptotic-like processes and complement-mediated pruning. As such, synaptosomes can be used as surrogate markers in synaptic pruning studies.

In adulthood, synaptic pruning optimizes learning capacity. At multiple time points from juvenile through adulthood, the most drastic changes in the number of immunoreactive synaptic boutons were observed in female rats between postnatal day (P) 35 and 45, aligned with the typical onset of puberty (Drzewiecki et. al, 2016). The puberty-induced synaptic pruning is observed across rodents of both sexes, likely orchestrated by changes in gonadal hormone levels (Simerly, 2002; Liu et al., 2012). Sex steroids abundant at puberty and during embryonic stages of sexual differentiation act as signaling molecules that interact with transcriptional regulators to guide sexually dimorphic neural circuit formation and synaptogenesis.

Synaptic pruning refines and restructures neural circuitry. The regulated removal of synaptic connections is vital in the prevention of neurodevelopmental disorders and

neurodegenerative diseases, such as Alzheimer's disease and schizophrenia (Sakai, 2020). During critical periods of neurodevelopment, synapse elimination is tightly controlled, and the dysregulation of this process leads to altered neural circuits. Excessive synaptic pruning is associated with early synaptic loss and increased plaque deposition characteristic of Alzheimer's disease (Hong et al., 2016). Similarly, the removal of synapses from glutamatergic excitatory pyramidal neurons in adolescence correlates with the onset of schizophrenia (Keshavan et al., 1994). Conversely, a deficit in pruning may lead to the overabundance of synapses, as observed in autism and neurodevelopmental delays (Xie et al., 2023; Beopoulous et al., 2022; Hansel, 2019).

Goals and Hypotheses

Given the consequences of a dysregulated pruning process, new protocols to understand the mechanisms that underlie synaptic pruning may advance therapeutic development. The ability to visualize and quantify synaptosomes, including their contents, provides a useful method to study various pruning-related diseases (Sellgren et al., 2019; Morini et al., 2021).

In an attempt to quantify the effects of puberty-mediated synaptic pruning in male rats, this study hypothesized that the cortical synaptosome quantity in pre-pubescent (P30) rats is greater than post-pubescent (P50) rats. This is based on the assumption that rats are juvenile through P45 when a surge in androgens characteristic of puberty is observed (Drzewiecki et al., 2016).

Animals

Young (P30) male Sprague-Dawley rats (n = 4, 23 days postnatal; Harlan, IN) and adult (P50) male Sprague-Dawley rats (n = 4, 43 days postnatal; Harlan, IN) and were

acclimated to their environment for 7 days following shipment before being subjected to tissue collection. The animals were housed in cages of 4, in a 12 h light: 12 h dark cycle at a constant temperature (23 ℃) with food and water available *ad libitum* according to the Association for Assessment and Accreditation of Laboratory Animal Care International.

4.2.3 The Effect of Ketamine on Synaptosomal Quantity in Rats

Introduction to Psychoplastogens as Potential Therapeutics for Cognitive Rehabilitation

Psychoplastogens are a class of compounds that include psychedelics, ketamine, and several other traditional, fast-acting antidepressants. These compounds act quickly to promote neuronal growth and enhance neuronal connectivity by activating and modulating biological targets, such as tropomyosin receptor kinase B (TrkB), the mammalian target of rapamycin (mTOR), and α-amino-3-hydroxy-5-methyl-4-isoxazolepropionic acid (AMPA) receptors (Kargbo, 2023; Vargas et al., 2021; Yang et al., 2013).

Psychological disorders are estimated to affect more than 20% of adults in the United States with varying forms and degrees of severity that impact their day-to-day lives, according to the National Institute of Mental Health. There has been a long-standing belief that psychological disorders such as depression, anxiety, and attention-deficit hyperactivity disorder (ADHD) result from ‘chemical imbalances’ in the brain (*Mental Health*, n.d.). The notion is that these conditions are caused by a disruption of neurotransmitter regulation and can be ‘fixed’ by introducing medications containing compounds or metabolites that increase or decrease certain neurotransmitters (Ang et. al,

2022). This chemical imbalance model is in contrast to a biopsychosocial model of psychological diseases, where disordered circuitry and function are caused by a combination of genetic, social and environmental factors that alter neurodevelopment on a molecular and cellular level (Deacon & Baird, 2009; Leo & Lacasse, 2008; Moncrieff et. al, 2022; Compton & Shim, 2015). The biopsychosocial model of psychiatric disease shifts the priority of interventions in development from medications that alter neurochemical levels to targeting neural circuit structure and function. Emerging therapeutics include non-invasive approaches, including electricity to modulate brain function, such as transcranial magnetic stimulation and deep brain stimulation (Scangos et al., 2023).

Novel approaches of psychoplastogen treatments could reverse disorder-related pathologies and promote neuroplasticity. With effects lasting up to months following a single administration likely due to changes in gene expression (Ly et al, 2018), the psychoplastogens can treat disorders including depression (Hibicke et al.,2020; Mandal et al., 2019; Barrett et al., 2020), post-traumatic stress disorder (PTSD) (Dunlap et al.,2018) and addiction (Bogenschutz & Johnson, 2016; Krupitsky et al, 2002). The psychoplastogens rewire neural circuitry via several mechanisms: metabolites act as agonists for serotonin receptors, as observed with the decreased activation of the brain's default mode network and desensitization of serotonin receptors under psychedelics (Stoliker et al., 2022; Damjanoska et al., 2004); as an antagonist of NMDAR, as observed in the antidepressant mechanisms of ketamine (Mandal et al., 2019); or increased synaptic levels of monoamines by traditional antidepressants (Vargas et al., 2021). The neuroplastic effects of psychoplastogens can be harnessed to increase the signaling of

regulatory proteins such as TrkB and growth factors such as brain-derived neurotrophic factor (BDNF) (Vargas et al., 2021).

In this thesis, the focus is on ketamine as an injectable, fast-acting dissociative anesthetic and its ability to help users 'detach' from their pain and environment. Beyond its antagonism of the NMDARs, its use as a therapeutic agent of psychological disorders relies on an ability to induce neuronal growth and cortical reorganization (Visser & Schug, 2006). Ketamine can repair maladaptive structural changes, such as the degeneration of synapses, dendritic spines and diminished dendritic arborization (Kargbo, 2023). A randomized, controlled trial by Singh et. al (2016) demonstrated ketamine's fast-acting antidepressant effects in patients with treatment-resistant depression when patients given twice or thrice-weekly doses of 0.5 mg/kg ketamine up to four weeks showed lower scores on the Montgomery-Åsberg Depression Rating Scale (MADRS) over 15 days after the last course. Patients who received the placebo maintained higher MADRS scores.

Goals and Hypotheses

This study investigated the effect of ketamine on synaptosomal quantity in rats to illustrate the effect of ketamine on synaptic growth.

Despite studies of ketamine's effects on neural circuitry, the use of synaptosomes remains novel in measuring the effects of psychoplastogenic compounds on the brain. This study hypothesized that at 48-hours post-injection, the cortices of rats given a single high-dose of 20 mg/kg ketamine have more synaptosomes compared to the rats given saline. Cortical synaptosomes were used because ketamine restored PFC neural function,

connectivity, and increased neurotransmission (Abdallah et. al, 2017; Li et. al, 2016; Kargbo, 2023).

Animals

Adult male Sprague-Dawley rats (n = 8, 6-7 weeks; Harlan, IN) were acclimated to their environment for 7 days following shipment before being subjected to ketamine injections. The animals were housed in cages of 4, in a 12 h light: 12 h dark cycle at a constant temperature (23 ℃) with food and water available *ad libitum* according to the Association for Assessment and Accreditation of Laboratory Animal Care International. During the acclimation period, each rat was handled for 10 minutes a day for a total of 3 days to minimize stress from being handled during the experimental process. The timeline of events is shown in **Figure 13**.

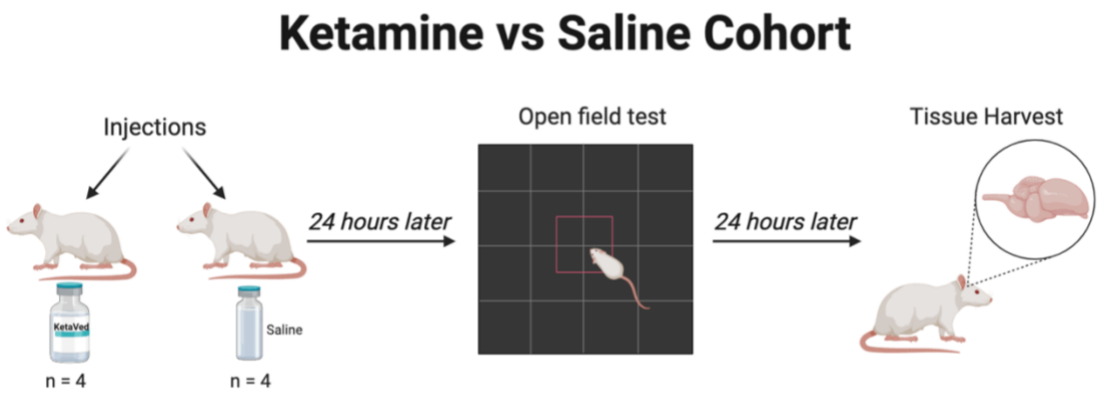

Figure 13 The timeline of events for rats in the ketamine vs saline cohort. Rats were randomly assigned to ketamine or saline injections (intraperitoneally). 24 hours later, rats were subjected to an open field test and the brain tissues were collected at 48 hours post-injection. Created with BioRender.com

Administration of Injections

Ketamine Hydrochloride (KetaVed Injection, 100 mg/mL, 10 mL) was purchased from Patterson Vet Supply (Greeley, CO). The stock drug solution was diluted in saline to a final concentration of 20 mg/mL. Rats were split into two groups of 4 animals and the ketamine group was given a single i.p. injection of 20 mg/mL ketamine while the control group was given equivalent volume of saline.

Open Field Task

At 24 hours post-injection, rats underwent an open field task to promote synaptic formation and neural changes associated with learning and memory and thus maximizing the effects of ketamine on neuroplasticity. The task took place in a room with white light at least an hour after a change in light cycle and ambient background white noise. In accordance with the setup used by Law et al. (2023), an open-box metal arena (69.215 cm x 69.215 cm) was used with a solid black plastic board floor. Each rat was given 15 minutes to explore the novel environment and all trials were video recorded using the EthoVision software (Noldus, Leesburg VA) to allow for movement tracking.

4.3 Tissue Preparation and Synaptic Flow Protocol

Rats were euthanized via an intraperitoneal (i.p.) overdose of sodium pentobarbital 7 DPI for the TBI cohort, 7 days upon arrival for the synaptic pruning cohort and 48 hours post-injection for the ketamine cohort. All rats were flushed with PBS (pH 6.8) for 6 minutes with the exception of P30 rats being flushed for 3 minutes until the livers cleared. The rats were then decapitated, and the brains were dissected into the left and right cortices, hippocampus, cerebellum, and the deep brain consisting of the remaining brain regions. These regions were snap-frozen on dry ice and stored at -80 ℃ until use.

For each synaptic flow run, a maximum of six samples were processed. In each run, at least one negative control sample containing only unstained synaptosomes was included. Samples were run in duplicate, with each run consisting of only the right or left cortex.

4.4 Approach to Result Analyses for All Experiments

The values for the mean and the standard deviation between sample replicates were grouped by and calculated for all four gating methods mentioned in **Section 2.1**. To identify significant outliers in the results, the variance value for each sample was calculated by dividing the standard deviation of the replicates by their mean. The maximum variance value of each gating strategy was used to split the data into decile bins and individual frequency distributions were used to determine where the majority of data lied for each of the gating methods. A comparison is then made between the four gating strategies and the one with lowest variance values was selected for further analysis.

To determine statistical significance, an online one-sample t-test calculator was used (https://www.graphpad.com/quickcalcs/oneSampleT1/). A one-sample t-test tests the hypothesis that a statistic of a list of numbers is equal to a chosen or known value, with an example being the testing of the hypothesis that the median of a set of numbers is equal to one (Wadhwa & Marappa-Ganeshan, 2023). In this study, the mean synaptosomal quantity of each experimental group was compared to a baseline value. The baseline value was calculated from the synaptosome quantity of all control groups: sham animals for the TBI experiment (n=4), P50 for the synaptic pruning experiment (n=4), saline for the ketamine experiment (n=4), control protocol development samples (n = 2).

4.5 Results

Flow cytometry dot plots were generated for each sample as described in **Section 2.2.** Minimal (<1%) events above 10^3 for the pre-synaptic and 10^4 for the post-synaptic markers were detected in samples containing only synaptosomes (no antibodies), which was used to set the gates for each experimental run.

The total events collected are shown on SSC-A vs FSC-A plots obtained from a representative sample of each treatment **(Figure 14**). From here, a polygon gate was drawn to isolate the middle portion of the 'comet'-like plot to select the P1 population; the P1 population represents the events that correlate to the size and granularity of synaptosomes set by the FSC and SSC values. The P1 population was drawn based on the SSC-A vs FSC-A plots of the negative controls (no antibody) for each experiment. The percentage of events in the P1 population ranged from 55.36% to 62.69% with an average negative control P1 population containing 58.91% and 59.63% for antibody-stained samples. From the 30,000 events collected, events in the P1 population corresponded to a range of 16,608 to 18,807 events displaying FSC and SSC values representing synaptosomes.

A t-test (https://www.graphpad.com/quickcalcs/ttest2/) revealed no significant differences between the P1 population percentage of negative controls and antibody-stained samples, suggesting that the main difference in synaptosomal counts was not observed during this stage of the analysis process. The P1 population was then plotted on a logarithmic scale of APC-A vs Alexa Fluor 488-A fluorescent intensity to determine the percent of events that co-express both pre- and post-synaptic markers. All four gating strategies mentioned in **Section 2.2** (Q2, Q2+Q4, negative-naught and floating) were

trialed. An example of the results generated using the negative-naught gating strategy is depicted below in **Figure 15**. A more detailed analysis of the results from each of the gating strategies will be presented in a later section. The antibody-stained samples showed a higher percentage of events that co-express both pre- and post-synaptic markers compared to the negative controls in all gating strategies.

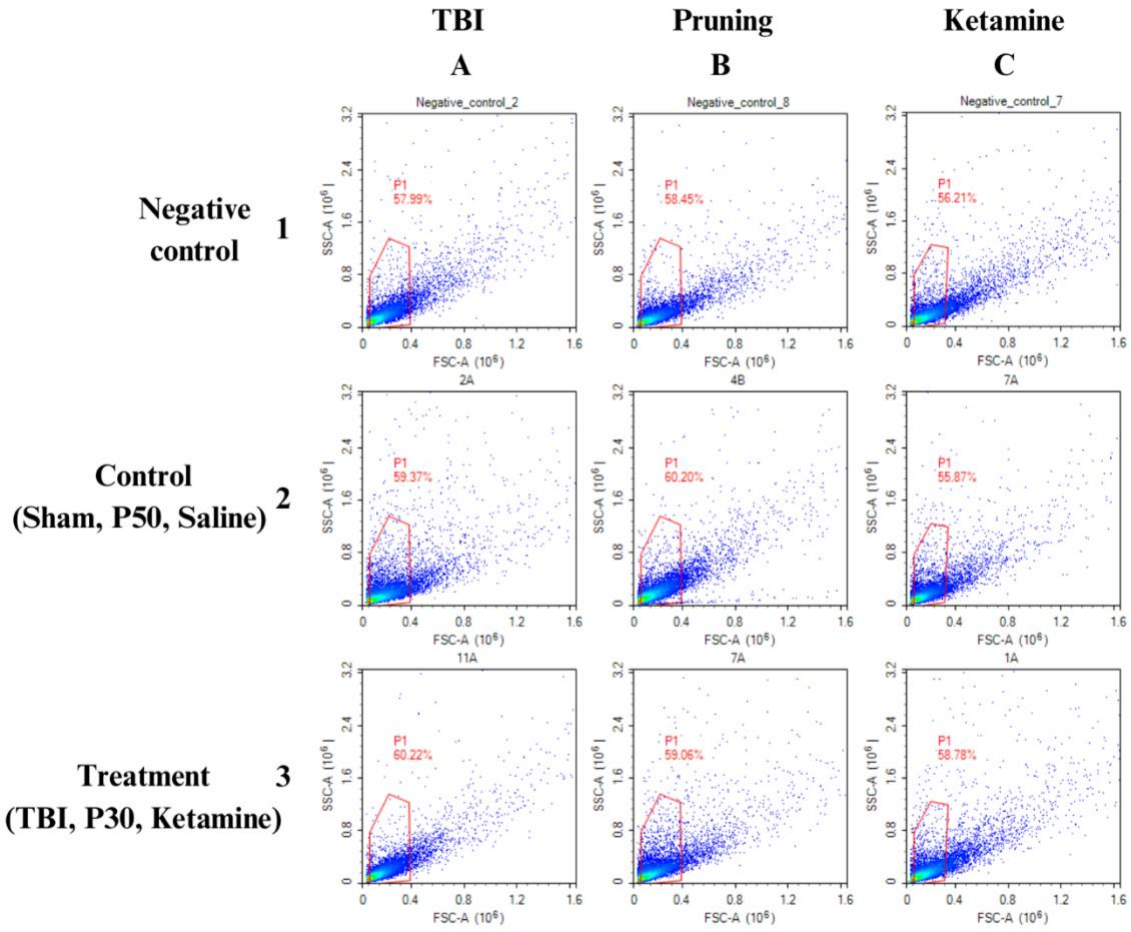

Figure 14 An example dot plot of SSC-A vs FSC-A of left cortical synaptosomes from which the P1 population was selected. All samples showed similar 'comet'-like distributions. The P1 population (in red) was selected from the negative controls of each

experiment (A1-C1), sham (A2), injured (A3), P50 (B2), P30 (B3) rats, saline (C2) and ketamine (C3) rats.

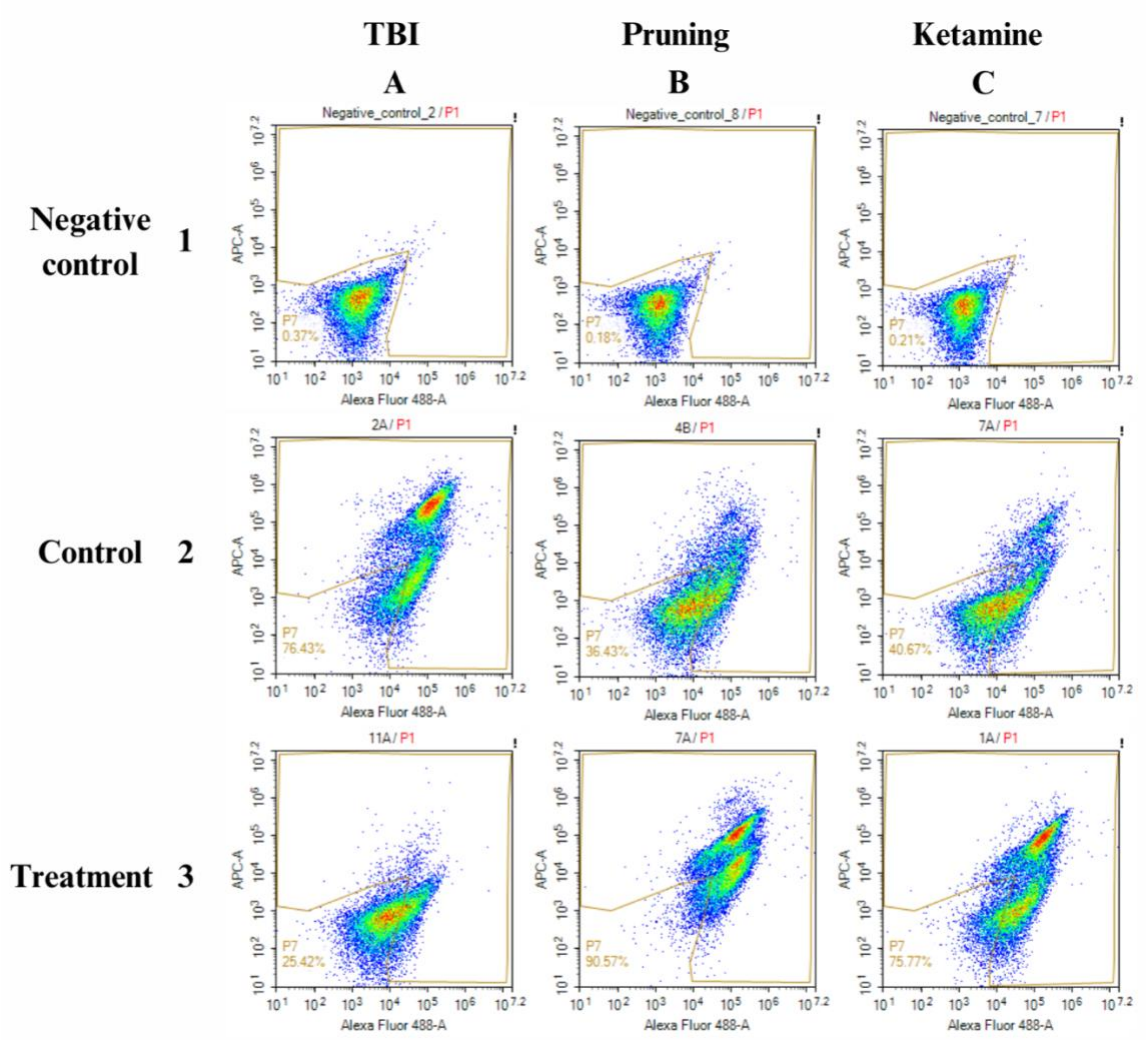

Figure 15 The logarithmic dot plot of APC-A (pre-synaptic marker) vs Alexa Fluor 488-A (post-synaptic marker) of the size-gated P1 population depicting left cortical synaptosomes. The negative-naught gating strategy (described in Section 2.2) was used to select the events outside of the population present in the negative control thereby excluding fluorescence signals from debris or events. The P7 population (in gold) was

selected from the negative controls of each experiment (A1-C1), sham(A2), injured (A3), P50 (B2), P30 (B3) rats, saline (C2) and ketamine (C3) rats.

For the replicates of each sample within the three experimental treatments, all four gating methods illustrated right-skewed frequency distributions. The floating population showed the highest mean variance and maximum variance value of 0.49 and 1.24, respectively; the Q2+Q4 population showed the least mean variance and maximum variance 0.13 and 0.40, respectively. The median values of variance between replicates were lower than the average values of variance in all four gating strategies, as shown in **Table 2**. This suggests a positively skewed distribution with increased possibility of significant outliers towards the higher end of the dataset. The Q2 population had the smallest range of variance with a value of 0.40 while the floating population showed the largest range of variance with a value of 1.22. The negative-naught and Q2+Q4 populations share a median value of 0.11, which was the lowest of all groups.

Table 2

Gating Strategy Statistics

	Q2	Q2+Q4	Negative-naught	Floating
Mean	0.32	0.13	0.16	0.49
Median	0.28	0.11	0.11	0.43
Standard Deviation	0.24	0.11	0.15	0.37
Minimum Value	7.23×10^{-3}	1.10×10^{-3}	1×10^{-6}	1.67×10^{-2}
Maximum Value	1.04	0.40	0.68	1.24

Note. The table above shows descriptive statistics (mean, median, standard deviation, minimum, and maximum values) of each gating strategy across all samples.

When the maximum variances of the sample replicates were divided into decile bins, the frequency distributions shown in **Figure 16** depict that a majority of the variation between replicates lie below 50% of the maximum variance. Out of 48 samples, the negative-naught gating method generated samples with the largest proportion of variance values being within 0 to 20% of the maximum variance (n=32), whereas the floating population gating method generated samples with the smallest proportion of variance values between 0 to 20% of the maximum (n=17). As such, the negative-naught gating method was selected to compare outcomes in different

treatments.

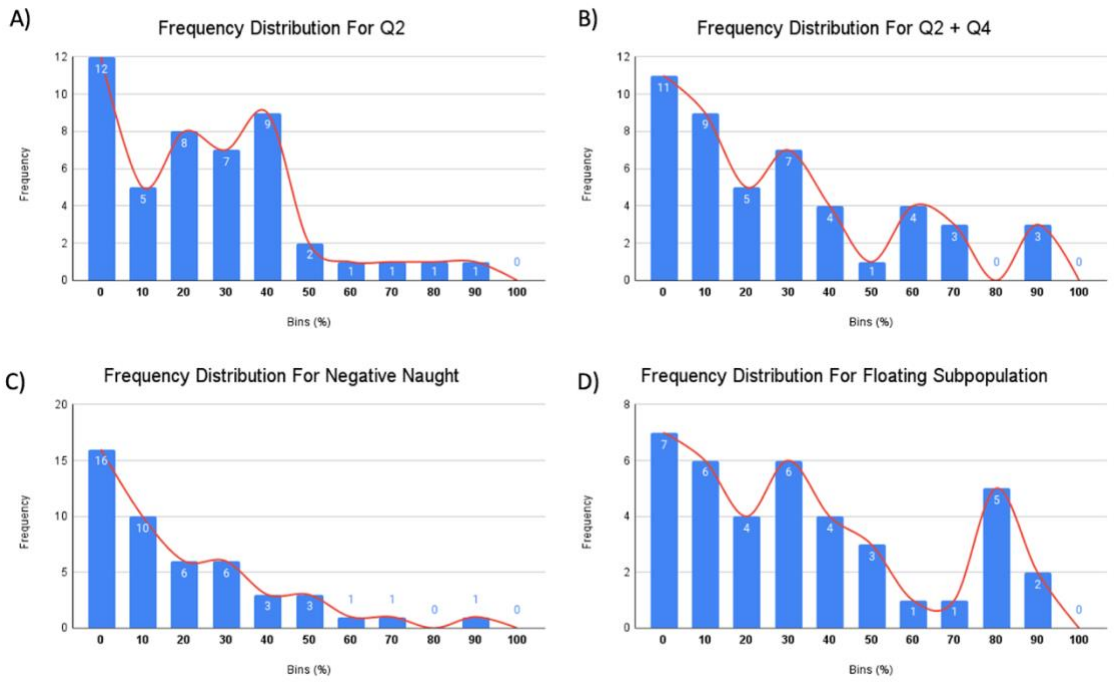

Figure 16 The frequency distributions of the variance in the (A) Q2 population alone, (B) Q2+Q4 population, (C) negative-naught population and (D) floating population when plotted against decile increments of the respective maximum values for each gating strategy.

For the baseline data used in the one-sample t-test, the average number of synaptosomes calculated from a pooled control group (n=27) was 8494.4. This value was compared to the average synaptosome counts of the TBI, P30 and ketamine groups; results are illustrated in **Table 3**. Amongst the three groups, the TBI (p=0.0005) and ketamine (p=0.0051) groups had significantly different synaptosome quantitities than the pooled control. The synaptosome count for the P30 group was not statistically significant from the control group (p=0.706).

Table 3
Results and Statistics

	Average Synaptosome Count	Standard Deviation	Number of Animals (n)	Number of Observations (n x 4)	p-value
Control Group	8494.4	11869.63	14	52*	N/A
TBI	5794.0	2431.57	4	16	0.0005
P30	9913.1	2744.69	4	16	0.706
Ketamine	9948.8	1773.20	4	16	0.0051

Note. The table above shows the average synaptosome count, standard deviation, number of animals and observations for the pooled control group and each of the experimental groups. The number of observations is multiplied by 4 to indicate the separation of the left and right hemispheres and include the two replicates for each animal. The p-value was generated using a one-sample t-test of the average synaptosome counts of the control group and each of the experimental groups. *The number of observations for the control group does not follow the nx4 pattern due to the inclusion of practice samples which were not run in duplicates.

CHAPTER 5

DISCUSSION

5.1 How the Findings Relate to Previous Studies and Methodology

Flow cytometry provides the ability to simultaneously quantify synaptosomes in large tissue samples. This is advantageous for the investigation of synaptic alterations, protein content and neurotransmitter profiles. This study's findings support the repeated use and validity of flow cytometry in synaptosomal quantification in neurodevelopmental, neurotrauma or neurodegeneration studies such as Alzheimer's and neuroinflammation (Gylys & Bilousova, 2017; Trebesova & Grilli, 2023; Györffy et al., 2018).

The quantification of synaptosomes in the TBI cohort generated average synaptosomal counts that were significantly less than the control group, supporting the study hypothesis that the cortical synaptosomes of TBI-rats would be decreased compared to uninjured rats at 7 days DPI. This could be due to neuroinflammation and neuronal atrophy and degeneration that occurs in response to injury, which is supported by the neuropathology at 7 DPI observed by Giordano et al. (2022). In accordance with this, a 35 to 45% reduction in the number of healthy neurons was seen alongside increased neuronal atrophy across all rat cortical layers at 7 DPI when compared to sham (Lifshitz & Lisenbee, 2012).

The average synaptosome quantity of P30 rats was not significantly different from the control group, indicating that the null hypothesis, which states that there are no differences between the synaptosomal quantities of P30 and P50 rats, cannot be rejected. The most parsimonious explanation for this discrepancy between the hypothesized effects

of adolescence-induced synaptic pruning on synaptosomal quantity is that the pruning process did not occur or is diminished in the P50 rats whereas the some of the P30 rats could have an earlier-than-expected pubertal onset. The range of puberty onset in male rats could have led to this phenomenon, with previous studies showing the period of pubertal onset to be between P40 to P60 (Drzewiecki et al., 2016; Koss et al., 2015; Fuochi et al., 2022). In rats, the preputial opening can be used as a marker of puberty onset due to the coincidental surge of androgens in male rats. However, the weight or age ranges are more accurate in measuring puberty onset in Sprague-Dawley rats (Fuochi et al., 2022). Since neither marker were measured in this study, the exact time of puberty for each P50 rat cannot be determined. As such, the possible inclusion of pre-pubescent P50 rats within the control group cannot be eliminated. Even if all P50 rats reached puberty prior to tissue harvest, the height of the pruning process might not have been reached, which could explain the absence of differences in synaptosome quantities between the two groups. The decreased synaptic loss could also be due to environmental influences and social interaction such as play behavior present in male, but not female, rats. Cortical synaptic pruning in female rats during puberty (P35 to P45) may be hormone-mediated, but likely influenced by play behavior in males. Koss et al. (2015) found that synaptic quantities in prepubertally-castrated and sham males were similar. This suggests that increased play behavior in males may impact neural reward circuits, potentially serving as a form of environmental enrichment that prevents neuronal loss and reduces the effects of synaptic pruning (Lima et al., 1998; Willing & Juraska, 2015). Alternatively, the limited sensitivity of the synaptic flow protocol could have minimized the detection of synaptic changes that occur during the pruning process (Hobson & Sims, 2019). To

mitigate the limited sensitivity of the synaptic flow protocol, alternative quantification methods involving Western blots or isotope-labeling can be used to complement current findings (McClatchy et al., 2007).

In the ketamine cohort, rats given a single high dose of ketamine showed significantly increased synaptosomal counts relative to the control group, including rats given saline. This aligns with the hypothesis of this study, which states that the cortical synaptosomes of rats given a single high dose of ketamine would show increased synaptosomal quantity compared to rats given saline. These findings are consistent with ketamine's ability to increase cortical synaptic protein expression and spine number as shown by Li et al. (2011) when measuring the effects of ketamine and on chronic stress-induced synaptic deficits. The increase in synaptosomes of ketamine rats relative to saline rats also support ketamine's rehabilitative properties as a rapid-acting antidepressant due to the increases in synapses and dendritic spines observed in subjects given ketamine. These effects are demonstrated by increased cortical glucose metabolism and global brain connectivity in patients with major depressive disorder who were given ketamine compared to controls (Li et al., 2016; Abdallah et al; 2017).

Since ketamine increases the growth of dendritic spines, rats were exposed to an open field arena 24 hours after injection as a form of novel stimulation to induce synapse formation and the reorganization of neural circuitry (Nithianantharajah et al., 2004). when mice were exposed to novel objects or areas, increased levels of the synaptophysin and PSD-95 suggested increased synaptic growth throughout the brain, which were not observed in control mice. A study by Novkovic et al. (2014) further supports this observation as mice placed in an enriched environment with constant novel stimulation

showed improved memory performance relative to control rats in a BDNF-dependent manner. This correlated with increased synaptic growth and neural rewiring associated with memory formation. Future studies could introduce more region-specific tasks or complex objects to enhance synaptic growth in other brain regions, such as the hippocampus or cerebellum.

5.2 Study Design and Protocol Limitations

Given the potential of the synaptic flow protocol, it is essential that the limitations and their postulated effects on this study's findings be identified for improvement in future use.

First of all, standardizing the samples to a protein concentration of 75 µg/mL could have been suboptimal, given that the pellet generated by a sample of that concentration was small, translucent and missed easily by the naked eye. While precautions were taken to ensure that only the supernatant was discarded during each wash step, human errors such as pipetting technique or physical limitations could have caused the disruption of the synaptosome-containing pellet, resulting in a number of synaptosomes being discarded. While the quality control process of the flow cytometer was conducted before every use, it does not reduce the possibility of synaptosomes clumping together, leading to coincident events, which could have led to fewer individual synaptosomes being detected (Hobson & Sims, 2019).

During the protocol adaptation process, difficulty in synaptosome-antibody binding, specifically with the pre-synaptic markers anti-Synapsin I and APC, was observed when comparing samples stained with one or both pre- and post-synaptic markers. During the protocol adaptation phase, there was minimal change in events

expressing the pre-synaptic marker when the different concentrations of pre-synaptic antibodies were manipulated. This contrasted with the proportional changes in events expressing the post-synaptic marker observed when it was manipulated. As Synapsin I is located within the pre-synaptic terminal compared to the location of PSD-95 as previously shown in **Figure 8**, this difference in position may have led to the discrepancies between the binding affinity of the pre- and post-synaptic antibodies. While the current protocol included partial fixation and permeabilization steps to minimize the effects of protein location on antibody binding, the incubation time or concentration of the permeabilization buffer (BD Cytofix/Cytoperm) used could have been suboptimal. To account for potential false negative events that were excluded from the Q2 gating strategy due to potential difficulties of the pre-synaptic antibodies binding to synaptosomes, the events collected in the Q4 population of the quadrant gate were included in synaptosomal quantification. However, this could also lead to the inclusion of false positives as there is no way to accurately distinguish between the events that are synaptosomes and non-synaptosomal particles. The former would be stained by a pre-synaptic marker, while the latter does not contain pre-synaptic proteins. To mitigate this, antibodies that bind to other pre-synaptic elements, such as Synaptophysin or SNAP-25, could be used in the protocol (Gylys et al., 2004; Gylys & Bilousova, 2017). Primary antibodies with conjugated fluorophores can also be used to optimize the staining and labeling of synaptosomes as it eliminates the use of secondary antibodies and thus increases staining specificity. The introduction of a step to block the Fc-receptors of non-synaptosomal particles has also been shown to be effective in reducing non-specific antibody-binding, consistent with the findings of Andersen et al (2016) when human immunoglobulin-G

(IgG) was used to block the Fc-receptors in reducing the non-specific staining of leukocytes used in flow cytometry.

In the validation experiments, the group sizes were kept small and only male animals were included. The small group size increased the susceptibility of findings to statistical outliers that result from biological variance. Furthermore, the samples were prepared in duplicates instead of triplicates, leaving out the possibility of removing significantly different results. This increased the possibility of error and biological variance which decreased the reliability of the findings. Therefore, the control groups of each experiment were pooled with samples from preliminary studies to form a control synaptosomal count for comparison. While the higher sample size decreases the influence of each sample and includes all possible data, the mean synaptosomal quantity is influenced by statistical outliers. Averaging the synaptosomal counts of both inter- and intra-animal samples could have reduced the observed effect sizes.

The results from the control group were pooled into a 'baseline' value to compare post-treatment changes. Comparisons were made using a one-sided t-test instead of an unpaired or paired t-test (Ross & Willson, 2017). Using a one-sample t-test for statistical analysis allowed for independent comparison between the mean of the pooled control and experimental groups. The pooled control group served as the true value as they were the combined measures from the untreated animals, which allowed a one-sided t-test to be used to measure changes in synaptosomal quantity incurred by each treatment for comparison to the initial, true value. However, since the comparison was for four independent groups, a one-sample t-test does not eliminate possibility of false positives (Type I errors) that increases by approximately 5% each time the control group is used.

This could lead to a significance level that is higher than suggested by the actual results, which could be mitigated by using a one-way analysis of variance (ANOVA). A one-way ANOVA compares the mean of three or more groups while accounting for potential Type I errors (Mishra et al., 2019). Since the control group in this study included the samples for the sham, P50, and saline rats which were used for repeated comparison against the independent treatments of TBI, P30, and ketamine rats, using a one-way ANOVA would minimize the error resulting from repeated use of the control value. The one-way ANOVA allows the mean of the control to be compared independently with all three treatments while keeping the chance for Type I error at 5% so that the p-values generated are not influenced by the number of t-tests conducted. As such, future studies could replace the one-sided t-test or combine both methods for more accurate analysis of results.

The current synaptosomal isolation protocol involves the homogenization of brain tissue with 0.32 M sucrose and a Teflon/glass Dounce homogenizer before centrifugation for separation of the synaptosomes and non-synaptosomal particles. While this protocol allows for rapid synaptosomal isolation without the need for subjecting samples in reagents of varying concentrations, the absence of a purification gradient during the synaptosomal isolation process could have contributed to larger standard deviations between sample replicates - especially in the P30 group. This may be due to non-synaptosomal particles remaining amongst the synaptosomes and thus increasing the possibility of non-specific antibody staining (Gylys & Bilousova, 2017). Synaptosomal purification was originally conducted by Gray & Whittaker (1962) during the isolation process using an isotonic sucrose gradient. Percoll gradients can also yield synaptosomes

with purities comparable to sucrose gradients in a shorter amount of time without interfering with biological assays (Dunkley & Robinson, 2018; Tenreiro et al., 2017). A Ficoll gradient can also be used in synaptosomal purification as it provides density without increasing osmotic pressure. Similar to Percoll gradients, the use of Ficoll requires less time relative to a sucrose gradient while increasing the synaptosomal homogeneity and viability (Booth & Clark, 1978; Dunkley & Robinson, 2018).

Compared to traditional methods used in synaptic and synaptosomal quantification, the synaptic flow protocol required a shorter time for antibody incubation and overall sample preparation. It also allows a large synaptosomal population to be quantified and their components simultaneously analyzed using different parameters while limiting the use of reagents such as DAB or silver. However, the spatial resolution of the synaptic flow data is limited compared to methods such as IHC or Timms-sulfide silver staining where synaptic contents can be visualized under a microscope for characterization (Whittaker, 1959; Claiborne et al., 1989). With IHC or Timms-sulfide silver staining where synaptic contents are stained and observed under an electron microscope, components such as synaptic density and the width of the synaptic cleft can be measured to observe the morphology of synapses. The synaptic flow protocol also does not verify the presence of specific pre- or post-synaptic proteins, which can instead be done using Western blots or mass spectrometry by comparing the molecular weights or mass-to-charge ratio of synaptosomal contents to those of previously known proteins and molecules. An example of such application is illustrated by Schrimpf et al. (2005) with the identification of molecules and proteins involved in signal transduction and

synaptic metabolism. The study used isotope-tagged synaptosomal proteins which were analyzed using tandem mass spectrometry to illustrate synaptosomal proteomics.

5.3 Areas for Further Study

With the adapted synaptic flow protocol, the areas of interest that could be explored include replication of the experiments conducted in this study on a larger scale, using more animals of both sexes to investigate potential differences between the responses of male and female rats. With female rats, the effects of the estrous cycle on synaptic pruning and synaptosomal counts could be measured to facilitate the current understanding of the neurological changes that occur with hormonal shifts. Combined with DNA or RNA sequencing methods, the genetic expression in synaptosomes can be determined to map the genomes of a specific synaptosomal population to further understand neurodegenerative diseases or neurological conditions (Di Paolo et al., 2021; Clifton et al, 2022). When investigating the role of the Parkin protein in Parkinson's-associated mitochondrial dysfunction, Lichter et al (2023) used DNA sequencing to find that the synaptosomes of Parkin-knockout mice showed reduced deleterious DNA mutations compared to mitochondrial mutator and Parkin-disinhibited mice. Mass spectrometry and electron microscopy can also be applied to synaptosomal studies for proteomic analysis and classification (Evans, 2015; Gulyássy et al., 2020; DiGiovanni et al., 2012).

The current protocol could also be used to quantify synaptosomes in the hippocampus, cerebellum, and brainstem (Dunkley & Robinson, 2018) to complement the findings of the cortex or in the investigation of region-specific effects (Ardalan et al., 2016; Postupna et al., 2018; Gylys et al., 2000). An example of this would be the use of a

similar synaptic flow protocol to investigate neurodegeneration-induced synaptic alterations in different brain regions. Postupna et al (2018) measured synaptosomal quantities and profiles in the hippocampi, cortices and striata of mice and post-mortem humans to observe the region-specific pathology associated with conditions such as Alzheimer's and Parkinson's.

To target and quantify inhibitory or excitatory circuits in the brain, the synaptic flow protocol could be modified to include antibodies that specifically bind to proteins present in inhibitory or excitatory synapses, such as GluR1 receptors or VGLUT1 (Krukowski et. al, 2021; Hobson & Sims, 2019). The changes in the number of synaptosomes containing inhibitory and excitatory proteins can illustrate the development of neural pathways throughout a certain period or stage of the neurodevelopmental process. The ability to quantify and characterize specific synaptosomal populations such as in dopamine transport can also be used when measuring the effects of certain behaviors or stimulation on the brain's reward pathway to inform addiction studies (Wells et al, 1999; Paget-Blanc et al., 2022). Furthermore, the synaptic flow technique can be developed to specifically target synaptosomes from axo-somatic or axo-dendritic synapses, which differ in morphology, size, and properties throughout the developmental process (Soghomonian et al, 2010). To hone in on the diverse roles of synapses in different parts of the CNS, the synaptosomes can represent the effects of development, insult, aging, and disease. This allows for a better understanding of the different mechanisms, properties and pathways involved in brain plasticity not just within the brain but also throughout the entire central nervous system.

REFERENCES

Abdallah, C. G., Averill, L. A., Collins, K. A., Geha, P., Schwartz, J., Averill, C., DeWilde, K. E., Wong, E., Anticevic, A., Tang, C. Y., Iosifescu, D. V., Charney, D. S., & Murrough, J. W. (2017). Ketamine Treatment and Global Brain Connectivity in Major Depression. *Neuropsychopharmacology*, *42*(6), Article 6. https://doi.org/10.1038/npp.2016.186

Ahmad, F., & Liu, P. (2020). Synaptosome as a tool in Alzheimer's disease research. *Brain Research*, *1746*, 147009. https://doi.org/10.1016/j.brainres.2020.147009

Allen, M. J., Sabir, S., & Sharma, S. (2023). GABA Receptor. In *StatPearls*. StatPearls Publishing. http://www.ncbi.nlm.nih.gov/books/NBK526124/

Andersen, M. N., Al-Karradi, S. N. H., Kragstrup, T. W., & Hokland, M. (2016). Elimination of erroneous results in flow cytometry caused by antibody binding to Fc receptors on human monocytes and macrophages. *Cytometry Part A*, *89*(11), 1001–1009. https://doi.org/10.1002/cyto.a.22995

Ang, B., Horowitz, M., & Moncrieff, J. (2022). Is the chemical imbalance an 'urban legend'? An exploration of the status of the serotonin theory of depression in the scientific literature. *SSM - Mental Health*, *2*, 100098. https://doi.org/10.1016/j.ssmmh.2022.100098

Ardalan, M., Wegener, G., Rafati, A. H., & Nyengaard, J. R. (2016). S-Ketamine Rapidly Reverses Synaptic and Vascular Deficits of Hippocampus in Genetic Animal Model of Depression. *International Journal of Neuropsychopharmacology*, *20*(3), 247–256. https://doi.org/10.1093/ijnp/pyw098

Baloyannis, S. J. (2015). Staining neurons with Golgi techniques in degenerative diseases of the brain. *Neural Regeneration Research*, *10*(5), 693–695. https://doi.org/10.4103/1673-5374.156950

Barrett, F. S., Doss, M. K., Sepeda, N. D., Pekar, J. J., & Griffiths, R. R. (2020). Emotions and brain function are altered up to one month after a single high dose of psilocybin. *Scientific Reports*, *10*, 2214. https://doi.org/10.1038/s41598-020-59282-y

Bennett, M. V. L., & Zukin, R. S. (2004). Electrical coupling and neuronal synchronization in the Mammalian brain. *Neuron*, *41*(4), 495–511. https://doi.org/10.1016/s0896-6273(04)00043-1

Beopoulos, A., Géa, M., Fasano, A., & Iris, F. (2022). Autism spectrum disorders pathogenesis: Toward a comprehensive model based on neuroanatomic and

neurodevelopment considerations. *Frontiers in Neuroscience*, *16*, 988735. https://doi.org/10.3389/fnins.2022.988735

Bogenschutz, M. P., & Johnson, M. W. (2016). Classic hallucinogens in the treatment of addictions. *Progress in Neuro-Psychopharmacology & Biological Psychiatry*, *64*, 250–258. https://doi.org/10.1016/j.pnpbp.2015.03.002

Booth, R. F., & Clark, J. B. (1978). A rapid method for the preparation of relatively pure metabolically competent synaptosomes from rat brain. *Biochemical Journal*, *176*(2), 365–370.

Bruyère, J., Abada, Y.-S., Vitet, H., Fontaine, G., Deloulme, J.-C., Cès, A., Denarier, E., Pernet-Gallay, K., Andrieux, A., Humbert, S., Potier, M.-C., Delatour, B., & Saudou, F. (2020). Presynaptic APP levels and synaptic homeostasis are regulated by Akt phosphorylation of huntingtin. *eLife*, *9*, e56371. https://doi.org/10.7554/eLife.56371

Chicurel, M., Terrian, D., & Potter, H. (1993). mRNA at the synapse: Analysis of a synaptosomal preparation enriched in hippocampal dendritic spines. *The Journal of Neuroscience*, *13*(9), 4054–4063. https://doi.org/10.1523/JNEUROSCI.13-09-04054.1993

Choquet, D., & Triller, A. (2013). The Dynamic Synapse. *Neuron*, *80*(3), 691–703. https://doi.org/10.1016/j.neuron.2013.10.013

Claiborne, B. J., Rea, M. A., & Terrian, D. M. (1989). Detection of zinc in isolated nerve terminals using a modified Timm's sulfide-silver method. *Journal of Neuroscience Methods*, *30*(1), 17–22. https://doi.org/10.1016/0165-0270(89)90069-1

Clifton, N. E., Bosworth, M. L., Haan, N., Rees, E., Holmans, P. A., Wilkinson, L. S., Isles, A. R., Collins, M. O., & Hall, J. (2022). Developmental disruption to the cortical transcriptome and synaptosome in a model of *SETD1A* loss-of-function. *Human Molecular Genetics*, *31*(18), 3095–3106. https://doi.org/10.1093/hmg/ddac105

Compton, M. T., & Shim, R. S. (2015). The Social Determinants of Mental Health. *FOCUS*, *13*(4), 419–425. https://doi.org/10.1176/appi.focus.20150017

Conrads, T. P., Alving, K., Veenstra, T. D., Belov, M. E., Anderson, G. A., Anderson, D. J., Lipton, M. S., Pasa-Tolić, L., Udseth, H. R., Chrisler, W. B., Thrall, B. D., & Smith, R. D. (2001). Quantitative analysis of bacterial and mammalian proteomes using a combination of cysteine affinity tags and 15N-metabolic labeling. *Analytical Chemistry*, *73*(9), 2132–2139. https://doi.org/10.1021/ac001487x

Damjanoska, K. J., Heidenreich, B. A., Kindel, G. H., D'Souza, D. N., Zhang, Y., Garcia, F., Battaglia, G., Wolf, W. A., Van de Kar, L. D., & Muma, N. A. (2004). Agonist-induced serotonin 2A receptor desensitization in the rat frontal cortex and hypothalamus. *The Journal of Pharmacology and Experimental Therapeutics*, *309*(3), 1043–1050. https://doi.org/10.1124/jpet.103.062067

Deacon, B. J., & Baird, G. L. (2009). The Chemical Imbalance Explanation of Depression: Reducing Blame at What Cost? *Journal of Social and Clinical Psychology*, *28*(4), 415–435. https://doi.org/10.1521/jscp.2009.28.4.415

DeCuypere, M., & Klimo, P. (2012). Spectrum of Traumatic Brain Injury from Mild to Severe. *Surgical Clinics of North America*, *92*(4), 939–957. https://doi.org/10.1016/j.suc.2012.04.005

DeFelipe, J., & Jones, E. G. (1992). Santiago Ramón y Cajal and methods in neurohistology,. *Trends in Neurosciences*, *15*(7), 237–246. https://doi.org/10.1016/0166-2236(92)90057-F

Di Paolo, A., Garat, J., Eastman, G., Farias, J., Dajas-Bailador, F., Smircich, P., & Sotelo-Silveira, J. R. (2021). Functional Genomics of Axons and Synapses to Understand Neurodegenerative Diseases. *Frontiers in Cellular Neuroscience*, *15*. https://www.frontiersin.org/articles/10.3389/fncel.2021.686722

DiGiovanni, J., Sun, T., & Sheng, Z.-H. (2012). Characterizing Synaptic Vesicle Proteins Using Synaptosomal Fractions and Cultured Hippocampal Neurons. *Current Protocols in Neuroscience / Editorial Board, Jacqueline N. Crawley ... [et Al.]*, *0 2*, Unit-2.722. https://doi.org/10.1002/0471142301.ns0207s59

D'Lauro, C., Johnson, B. R., McGinty, G., Allred, C. D., Campbell, D. E., & Jackson, J. C. (2018). Reconsidering Return-to-Play Times: A Broader Perspective on Concussion Recovery. *Orthopaedic Journal of Sports Medicine*, *6*(3), 2325967118760854. https://doi.org/10.1177/2325967118760854

Dowdall, M. J. (1975). Synthesis and Storage of Acetylcholine in Cholinergic Nerve Terminals. In S. Berl, D. D. Clarke, & D. Schneider (Eds.), *Metabolic Compartmentation and Neurotransmission: Relation to Brain Structure and Function* (pp. 585–607). Springer US. https://doi.org/10.1007/978-1-4613-4319-6_36

Drzewiecki, C. M., Willing, J., & Juraska, J. M. (2016). Synaptic number changes in the medial prefrontal cortex across adolescence in male and female rats: A role for pubertal onset. *Synapse (New York, N.Y.)*, *70*(9), 361–368. https://doi.org/10.1002/syn.21909

Dunkley, P. R., & Robinson, P. J. (2018). Synaptosome Preparations: Which Procedure Should I Use? In K. M. Murphy (Ed.), *Synaptosomes* (pp. 27–53). Springer. https://doi.org/10.1007/978-1-4939-8739-9_3

Dunlap, L. E., Andrews, A. M., & Olson, D. E. (2018). Dark Classics in Chemical Neuroscience: 3,4-Methylenedioxymethamphetamine. *ACS Chemical Neuroscience*, *9*(10), 2408–2427. https://doi.org/10.1021/acschemneuro.8b00155

Edlow, B. L., Copen, W. A., Izzy, S., Bakhadirov, K., van der Kouwe, A., Glenn, M. B., Greenberg, S. M., Greer, D. M., & Wu, O. (2016). Diffusion tensor imaging in acute-to-subacute traumatic brain injury: A longitudinal analysis. *BMC Neurology*, *16*, 2. https://doi.org/10.1186/s12883-015-0525-8

El-Hajjar, L., Ali Ahmad, F., & Nasr, R. (2023). A Guide to Flow Cytometry: Components, Basic Principles, Experimental Design, and Cancer Research Applications. *Current Protocols*, *3*(3), e721. https://doi.org/10.1002/cpz1.721

Evans, G. J. O. (2015a). Subcellular Fractionation of the Brain: Preparation of Synaptosomes and Synaptic Vesicles. *Cold Spring Harbor Protocols*, *2015*(5), pdb.prot083469. https://doi.org/10.1101/pdb.prot083469

Evans, G. J. O. (2015b). The Synaptosome as a Model System for Studying Synaptic Physiology. *Cold Spring Harbor Protocols*, *2015*(5), pdb.top074450. https://doi.org/10.1101/pdb.top074450

Faust, T., Gunner, G., & Schafer, D. P. (2021). Mechanisms governing activity-dependent synaptic pruning in the mammalian CNS - PMC. *Nature Reviews Neuroscience*. https://doi.org/10.1038%2Fs41583-021-00507-y

Fuochi, S., Galasso, M. E., Colombo, Ri., Giaquinto, D., Girolamo, P., & D'Angelo, L. (2022). *Puberty onset curve in CD (Sprague Dawley) and Long Evans outbred male rats—Sara Fuochi, Marica E Galasso, Rita Colombo, Daniela Giaquinto, Paolo De Girolamo, Livia D'Angelo, 2022*. https://journals.sagepub.com/doi/10.1177/00236772221078725?url_ver=Z39.88-2003&rfr_id=ori:rid:crossref.org&rfr_dat=cr_pub%20%200pubmed

Giordano, K. R., Law, L. M., Henderson, J., Rowe, R. K., & Lifshitz, J. (2022). Time Course of Remote Neuropathology Following Diffuse Traumatic Brain Injury in the Male Rat. *Experimental Neurobiology*, *31*(2), 105–115. https://doi.org/10.5607/en21027

Giordano, K. R., & Lifshitz, J. (2021). Pathophysiology of Traumatic Brain Injury. In S. Honeybul & A. G. Kolias (Eds.), *Traumatic Brain Injury: Science, Practice, Evidence and Ethics* (pp. 13–18). Springer International Publishing. https://doi.org/10.1007/978-3-030-78075-3_2

Golden, J. P., Justin, G. A., Nasir, M., & Ligler, F. S. (2012). Hydrodynamic focusing – a versatile tool. *Analytical and Bioanalytical Chemistry*, *402*(1), 325–335. https://doi.org/10.1007/s00216-011-5415-3

Graham, N. S., Cole, J. H., Bourke, N. J., Schott, J. M., & Sharp, D. J. (2023). Distinct patterns of neurodegeneration after TBI and in Alzheimer's disease—Graham—2023—Alzheimer's & Dementia—Wiley Online Library. *The Journal of the Alzheimer's Association*. https://doi.org/10.1002/alz.12934

Graham, N. S., & Sharp, D. J. (2019). Understanding neurodegeneration after traumatic brain injury: From mechanisms to clinical trials in dementia. *Journal of Neurology, Neurosurgery & Psychiatry*, *90*(11), 1221–1233. https://doi.org/10.1136/jnnp-2017-317557

Gray, E. G., & Whittaker, V. P. (1962). The isolation of nerve endings from brain: An electron-microscopic study of cell fragments derived by homogenization and centrifugation. *Journal of Anatomy*, *96*(Pt 1), 79–88.

Gulyássy, P., Puska, G., Györffy, B. A., Todorov-Völgyi, K., Juhász, G., Drahos, L., & Kékesi, K. A. (2020). Proteomic comparison of different synaptosome preparation procedures. *Amino Acids*, *52*(11), 1529–1543. https://doi.org/10.1007/s00726-020-02912-6

Gylys, K. H., & Bilousova, T. (2017). Flow Cytometry Analysis and Quantitative Characterization of Tau in Synaptosomes from Alzheimer's Disease Brains. *Methods in Molecular Biology (Clifton, N.J.)*, *1523*, 273–284. https://doi.org/10.1007/978-1-4939-6598-4_16

Gylys, K. H., Fein, J. A., & Cole, G. M. (2000). Quantitative characterization of crude synaptosomal fraction (P-2) components by flow cytometry. *Journal of Neuroscience Research*, *61*(2), 186–192. https://doi.org/10.1002/1097-4547(20000715)61:2<186::AID-JNR9>3.0.CO;2-X

Gylys, K. H., Fein, J. A., Yang, F., & Cole, G. M. (2004). Enrichment of presynaptic and postsynaptic markers by size-based gating analysis of synaptosome preparations from rat and human cortex. *Cytometry Part A*, *60A*(1), 90–96. https://doi.org/10.1002/cyto.a.20031

Györffy, B. A., Kun, J., Török, G., Bulyáki, É., Borhegyi, Z., Gulyássy, P., Kis, V., Szocsics, P., Micsonai, A., Matkó, J., Drahos, L., Juhász, G., Kékesi, K. A., & Kardos, J. (2018). Local apoptotic-like mechanisms underlie complement-mediated synaptic pruning. *Proceedings of the National Academy of Sciences of the United States of America*, *115*(24), 6303–6308. https://doi.org/10.1073/pnas.1722613115

Hansel, C. (2019). Deregulation of synaptic plasticity in autism. *Neuroscience Letters*, *688*, 58–61. https://doi.org/10.1016/j.neulet.2018.02.003

Hebb, C. O., & Whittaker, V. P. (1958). Intracellular distributions of acetylcholine and choline acetylase. *The Journal of Physiology*, *142*(1), 187–196. https://doi.org/10.1113/jphysiol.1958.sp006008

Henny, P., Brischoux, F., Mainville, L., Stroh, T., & Jones, B. E. (2010). Immunohistochemical evidence for synaptic release of glutamate from orexin terminals in the locus coeruleus. *Neuroscience*, *169*(3), 1150–1157. https://doi.org/10.1016/j.neuroscience.2010.06.003

Hibicke, M., Landry, A. N., Kramer, H. M., Talman, Z. K., & Nichols, C. D. (2020). Psychedelics, but Not Ketamine, Produce Persistent Antidepressant-like Effects in a Rodent Experimental System for the Study of Depression. *ACS Chemical Neuroscience*, *11*(6), 864–871. https://doi.org/10.1021/acschemneuro.9b00493

Hobson, B. D., & Sims, P. A. (2019). Critical Analysis of Particle Detection Artifacts in Synaptosome Flow Cytometry. *eNeuro*, *6*(3), ENEURO.0009-19.2019. https://doi.org/10.1523/ENEURO.0009-19.2019

Hong, S., Beja-Glasser, V. F., Nfonoyim, B. M., Frouin, A., Li, S., Ramakrishnan, S., Merry, K. M., Shi, Q., Rosenthal, A., Barres, B. A., Lemere, C. A., Selkoe, D. J., & Stevens, B. (2016). Complement and microglia mediate early synapse loss in Alzheimer mouse models. *Science*, *352*(6286), 712–716. https://doi.org/10.1126/science.aad8373

Hsia, A., Masliah, E., McConlogue, L., & Mucke, L. (1999). Plaque-independent disruption of neural circuits in Alzheimer's disease mouse models | PNAS. *PNAS*, *96*(6). https://www.pnas.org/doi/full/10.1073/pnas.96.6.3228

Hubel, D. H., Wiesel, T. N., & LeVay, S. (1977). Plasticity of Ocular Dominance Columns in Monkey Striate Cortex. *Philosophical Transactions of the Royal Society of London. Series B, Biological Sciences*, *278*(961), 377–409.

Hunt, D. L., & Castillo, P. E. (2012). Synaptic plasticity of NMDA receptors: Mechanisms and functional implications. *Current Opinion in Neurobiology*, *22*(3), 496–508. https://doi.org/10.1016/j.conb.2012.01.007

Iverson, G. L., Gardner, A. J., Terry, D. P., Ponsford, J. L., Sills, A. K., Broshek, D. K., & Solomon, G. S. (2017). Predictors of clinical recovery from concussion: A systematic review. *British Journal of Sports Medicine*, *51*(12), 941–948. https://doi.org/10.1136/bjsports-2017-097729

Kargbo, R. B. (2023). Psychoplastogens: A Novel Therapeutic Approach for Neurological Diseases and Disorders. *ACS Medicinal Chemistry Letters*, *14*(9), 1144–1145. https://doi.org/10.1021/acsmedchemlett.3c00309

Keshavan, M. S., Anderson, S., & Pettegrew, J. W. (1994). Is schizophrenia due to excessive synaptic pruning in the prefrontal cortex? The Feinberg hypothesis revisited. *Journal of Psychiatric Research*, *28*(3), 239–265. https://doi.org/10.1016/0022-3956(94)90009-4

Kim, S.-W., Roh, J., & Park, C.-S. (2016). Immunohistochemistry for Pathologists: Protocols, Pitfalls, and Tips. *Journal of Pathology and Translational Medicine*, *50*(6), 411–418. https://doi.org/10.4132/jptm.2016.08.08

Koss, W. A., Lloyd, M. M., Sadowski, R. N., Wise, L. M., & Juraska, J. M. (2015). Gonadectomy before puberty Increases the number of neurons and glia in the medial prefrontal cortex of female, but not male, rats. *Developmental Psychobiology*, *57*(3), 305–312. https://doi.org/10.1002/dev.21290

Krukowski, K., Grue, K., Becker, M., Elizarraras, E., Frias, E. S., Halvorsen, A., Koenig-Zanoff, M., Frattini, V., Nimmagadda, H., Feng, X., Jones, T., Nelson, G., Ferguson, A. R., & Rosi, S. (2021). The impact of deep space radiation on cognitive performance: From biological sex to biomarkers to countermeasures. *Science Advances*, *7*(42), eabg6702. https://doi.org/10.1126/sciadv.abg6702

Krupitsky, E., Burakov, A., Romanova, T., Dunaevsky, I., Strassman, R., & Grinenko, A. (2002). Ketamine psychotherapy for heroin addiction: Immediate effects and two-year follow-up. *Journal of Substance Abuse Treatment*, *23*(4), 273–283. https://doi.org/10.1016/s0740-5472(02)00275-1

Law, L. M., Griffiths, D. R., & Lifshitz, J. (2023). Peg Forest Rehabilitation – A novel spatial navigation based cognitive rehabilitation paradigm for experimental neurotrauma. *Behavioural Brain Research*, *443*, 114355. https://doi.org/10.1016/j.bbr.2023.114355

Leddy, J. J., Haider, M. N., Hinds, A. L., Darling, S., & Willer, B. S. (2019). A Preliminary Study of the Effect of Early Aerobic Exercise Treatment for Sport-Related Concussion in Males. *Clinical Journal of Sport Medicine : Official Journal of the Canadian Academy of Sport Medicine*, *29*(5), 353–360. https://doi.org/10.1097/JSM.0000000000000663

Leo, J., & Lacasse, J. R. (2008). The Media and the Chemical Imbalance Theory of Depression. *Society*, *45*(1), 35–45. https://doi.org/10.1007/s12115-007-9047-3

Letellier, M., Levet, F., Thoumine, O., & Goda, Y. (2019). Differential role of pre- and postsynaptic neurons in the activity-dependent control of synaptic strengths across

dendrites. *PLoS Biology*, *17*(6), e2006223. https://doi.org/10.1371/journal.pbio.2006223

Levy, W. B., Redburn, D. A., & Cotman, C. W. (1973). Stimulus-Coupled Secretion of γ-Aminobutyric Acid from Rat Brain Synaptosomes. *Science*, *181*(4100), 676–678. https://doi.org/10.1126/science.181.4100.676

Li, C.-T., Chen, M.-H., Lin, W.-C., Hong, C.-J., Yang, B.-H., Liu, R.-S., Tu, P.-C., & Su, T.-P. (2016). The effects of low-dose ketamine on the prefrontal cortex and amygdala in treatment-resistant depression: A randomized controlled study. *Human Brain Mapping*, *37*(3), 1080–1090. https://doi.org/10.1002/hbm.23085

Li, L., Chin, L. S., Shupliakov, O., Brodin, L., Sihra, T. S., Hvalby, O., Jensen, V., Zheng, D., McNamara, J. O., & Greengard, P. (1995). Impairment of synaptic vesicle clustering and of synaptic transmission, and increased seizure propensity, in synapsin I-deficient mice. *Proceedings of the National Academy of Sciences of the United States of America*, *92*(20), 9235–9239.

Li, N., Liu, R.-J., Dwyer, J. M., Banasr, M., Lee, B., Son, H., Li, X.-Y., Aghajanian, G., & Duman, R. S. (2011). Glutamate N-methyl-D-aspartate Receptor Antagonists Rapidly Reverse Behavioral and Synaptic Deficits Caused by Chronic Stress Exposure. *Biological Psychiatry*, *69*(8), 754–761. https://doi.org/10.1016/j.biopsych.2010.12.015

Libard, S., Cerjan, D., & Alafuzoff, I. (2019). Characteristics of the tissue section that influence the staining outcome in immunohistochemistry. *Histochemistry and Cell Biology*, *151*(1), 91–96. https://doi.org/10.1007/s00418-018-1742-1

Lichter, E. Z., Trease, A. J., Cooper, K., Stauch, K. L., & Fox, H. S. (2023). Effects of Parkin on the Mitochondrial Genome in the Heart and Brain of Mitochondrial Mutator Mice. *Advanced Biology*, *7*(8), 2300154. https://doi.org/10.1002/adbi.202300154

Lifshitz, J., & Lisembee, A. M. (2012). Neurodegeneration in the somatosensory cortex after experimental diffuse brain injury. *Brain Structure & Function*, *217*(1), 49–61. https://doi.org/10.1007/s00429-011-0323-z

Lifshitz, J., Rowe, R. K., Griffiths, D. R., Evilsizor, M. N., Thomas, T. C., Adelson, P. D., & McIntosh, T. K. (2016). Clinical relevance of midline fluid percussion brain injury: Acute deficits, chronic morbidities, and the utility of biomarkers. *Brain Injury*, *30*(11), 1293–1301. https://doi.org/10.1080/02699052.2016.1193628

Lima, J. G., de Oliveira, L. M., & Almeida, S. S. (1998). Effects of Early Concurrent Protein Malnutrition and Environmental Stimulation on the Central Nervous System

and Behavior. *Nutritional Neuroscience*, *1*(6), 439–448. https://doi.org/10.1080/1028415X.1998.11747254

Liu, Y., Rutlin, M., Huang, S., Barrick, C. A., Wang, F., Jones, K. R., Tessarollo, L., & Ginty, D. D. (2012). Sexually Dimorphic BDNF Signaling Directs Sensory Innervation of the Mammary Gland. *Science*. https://doi.org/10.1126/science.1228258

Ly, C., Greb, A. C., Cameron, L. P., Wong, J. M., Barragan, E. V., Wilson, P. C., Burbach, K. F., Zarandi, S. S., Sood, A., Paddy, M. R., Duim, W. C., Dennis, M. Y., McAllister, A. K., Ori-McKenney, K. M., Gray, J. A., & Olson, D. E. (2018). Psychedelics Promote Structural and Functional Neural Plasticity. *Cell Reports*, *23*(11), 3170–3182. https://doi.org/10.1016/j.celrep.2018.05.022

Maas, A. I. R., Menon, D. K., Adelson, P. D., Andelic, N., Bell, M. J., Belli, A., Bragge, P., Brazinova, A., Büki, A., Chesnut, R. M., Citerio, G., Coburn, M., Cooper, D. J., Crowder, A. T., Czeiter, E., Czosnyka, M., Diaz-Arrastia, R., Dreier, J. P., Duhaime, A.-C., … InTBIR Participants and Investigators. (2017). Traumatic brain injury: Integrated approaches to improve prevention, clinical care, and research. *The Lancet. Neurology*, *16*(12), 987–1048. https://doi.org/10.1016/S1474-4422(17)30371-X

Mac Donald, C. L., Dikranian, K., Song, S. K., Bayly, P. V., Holtzman, D. M., & Brody, D. L. (2007). Detection of Traumatic Axonal Injury with Diffusion Tensor Imaging in a Mouse Model of Traumatic Brain Injury. *Experimental Neurology*, *205*(1), 116–131. https://doi.org/10.1016/j.expneurol.2007.01.035

Maeda, T., Lee, S. M., & Hovda, D. A. (2005). Restoration of cerebral vasoreactivity by an L-type calcium channel blocker following fluid percussion brain injury. *Journal of Neurotrauma*, *22*(7), 763–771. https://doi.org/10.1089/neu.2005.22.763

Magaki, S., Hojat, S. A., Wei, B., So, A., & Yong, W. H. (2019). An Introduction to the Performance of Immunohistochemistry. *Methods in Molecular Biology (Clifton, N.J.)*, *1897*, 289–298. https://doi.org/10.1007/978-1-4939-8935-5_25

Mahmood, T., & Yang, P.-C. (2012). Western Blot: Technique, Theory, and Trouble Shooting. *North American Journal of Medical Sciences*, *4*(9), 429–434. https://doi.org/10.4103/1947-2714.100998

Maksimovic, S., Useinovic, N., Quillinan, N., Covey, D. F., Todorovic, S. M., & Jevtovic-Todorovic, V. (2022). General Anesthesia and the Young Brain: The Importance of Novel Strategies with Alternate Mechanisms of Action. *International Journal of Molecular Sciences*, *23*(3), Article 3. https://doi.org/10.3390/ijms23031889

Mandal, S., Sinha, V. K., & Goyal, N. (2019). Efficacy of ketamine therapy in the treatment of depression. *Indian Journal of Psychiatry*, *61*(5), 480–485. https://doi.org/10.4103/psychiatry.IndianJPsychiatry_484_18

McClatchy, D. B., Liao, L., Park, S. K., Venable, J. D., & Yates, J. R. (2007). Quantification of the synaptosomal proteome of the rat cerebellum during post-natal development. *Genome Research*, *17*(9), 1378–1388. https://doi.org/10.1101/gr.6375007

MCKEE, A. C., & DANESHVAR, D. H. (2015). The neuropathology of traumatic brain injury. *Handbook of Clinical Neurology*, *127*, 45–66. https://doi.org/10.1016/B978-0-444-52892-6.00004-0

McKinnon, K. M. (2018). Flow Cytometry: An Overview. *Current Protocols in Immunology*, *120*, 5.1.1-5.1.11. https://doi.org/10.1002/cpim.40

Mental Health: A Report of the Surgeon General. (n.d.). Reports of the Surgeon General - Profiles in Science. Retrieved October 2, 2023, from https://profiles.nlm.nih.gov/spotlight/nn/catalog/nlm:nlmuid-101584932X120-doc

Mental Illness. (n.d.). National Institute of Mental Health (NIMH). Retrieved October 2, 2023, from https://www.nimh.nih.gov/health/statistics/mental-illness

Mirza, F. J., & Zahid, S. (2018). The Role of Synapsins in Neurological Disorders. *Neuroscience Bulletin*, *34*(2), 349–358. https://doi.org/10.1007/s12264-017-0201-7

Moncrieff, J., Cooper, R. E., Stockmann, T., Amendola, S., Hengartner, M. P., & Horowitz, M. A. (2022). The serotonin theory of depression: A systematic umbrella review of the evidence. *Molecular Psychiatry*, 1–14. https://doi.org/10.1038/s41380-022-01661-0

Mora, N., & Rosales, C. (2009). [Fc receptor functions in host and immune regulation]. *Revista De Investigacion Clinica; Organo Del Hospital De Enfermedades De La Nutricion*, *61*(4), 313–326.

Moreno, V., Smith, E. A., & Piña-Oviedo, S. (2022). Fluorescent Immunohistochemistry. *Methods in Molecular Biology (Clifton, N.J.)*, *2422*, 131–146. https://doi.org/10.1007/978-1-0716-1948-3_9

Moretti, L., Cristofori, I., Weaver, S. M., Chau, A., Portelli, J. N., & Grafman, J. (2012). Cognitive decline in older adults with a history of traumatic brain injury. *The Lancet Neurology*, *11*(12), 1103–1112. https://doi.org/10.1016/S1474-4422(12)70226-0

Morini, R., Bizzotto, M., Perrucci, F., Filipello, F., & Matteoli, M. (2021). Strategies and Tools for Studying Microglial-Mediated Synapse Elimination and Refinement.

Frontiers in Immunology, *12*. https://www.frontiersin.org/articles/10.3389/fimmu.2021.640937

Navlakha, S., Barth, A. L., & Bar-Joseph, Z. (2015). Decreasing-Rate Pruning Optimizes the Construction of Efficient and Robust Distributed Networks. *PLoS Computational Biology*, *11*(7), e1004347. https://doi.org/10.1371/journal.pcbi.1004347

Neely, G. A., Sabir, S., & Kohli, A. (2023). Neostigmine. In *StatPearls*. StatPearls Publishing. http://www.ncbi.nlm.nih.gov/books/NBK470596/

Nithianantharajah, J., Levis, H., & Murphy, M. (2004). Environmental enrichment results in cortical and subcortical changes in levels of synaptophysin and PSD-95 proteins. *Neurobiology of Learning and Memory*, *81*(3), 200–210. https://doi.org/10.1016/j.nlm.2004.02.002

Novkovic, T., Mittmann, T., & Manahan-Vaughan, D. (2015). BDNF contributes to the facilitation of hippocampal synaptic plasticity and learning enabled by environmental enrichment. *Hippocampus*, *25*(1), 1–15. https://doi.org/10.1002/hipo.22342

Oda, Y., Huang, K., Cross, F. R., Cowburn, D., & Chait, B. T. (1999). Accurate quantitation of protein expression and site-specific phosphorylation. *Proceedings of the National Academy of Sciences of the United States of America*, *96*(12), 6591–6596.

Osimo, E. F., Beck, K., Reis Marques, T., & Howes, O. D. (2019). Synaptic loss in schizophrenia: A meta-analysis and systematic review of synaptic protein and mRNA measures. *Molecular Psychiatry*, *24*(4), Article 4. https://doi.org/10.1038/s41380-018-0041-5

Paget-Blanc, V., Pfeffer, M. E., Pronot, M., Lapios, P., Angelo, M.-F., Walle, R., Cordelières, F. P., Levet, F., Claverol, S., Lacomme, S., Petrel, M., Martin, C., Pitard, V., De Smedt Peyrusse, V., Biederer, T., Perrais, D., Trifilieff, P., & Herzog, E. (2022). A synaptomic analysis reveals dopamine hub synapses in the mouse striatum. *Nature Communications*, *13*, 3102. https://doi.org/10.1038/s41467-022-30776-9

Paolicelli, R. C., Bolasco, G., Pagani, F., Maggi, L., Scianni, M., Panzanelli, P., Giustetto, M., Ferreira, T. A., Guiducci, E., Dumas, L., Ragozzino, D., & Gross, C. T. (2011). Synaptic pruning by microglia is necessary for normal brain development. *Science (New York, N.Y.)*, *333*(6048), 1456–1458. https://doi.org/10.1126/science.1202529

Park, E., Cho, M., & Ki, C.-S. (2009). Correct use of repeated measures analysis of variance. *The Korean Journal of Laboratory Medicine*, *29*(1), 1–9. https://doi.org/10.3343/kjlm.2009.29.1.1

Peters, A. J., Villasana, L. E., & Schnell, E. (2018). Ketamine alters hippocampal cell proliferation and improves learning in mice after traumatic brain injury. *Anesthesiology*, *129*(2), 278–295. https://doi.org/10.1097/ALN.0000000000002197

Picone, P., Porcelli, G., Bavisotto, C. C., Nuzzo, D., Galizzi, G., Biagio, P. L. S., Bulone, D., & Di Carlo, M. (2021). Synaptosomes: New vesicles for neuronal mitochondrial transplantation. *Journal of Nanobiotechnology*, *19*(1), 6. https://doi.org/10.1186/s12951-020-00748-6

Picot, J., Guerin, C. L., Le Van Kim, C., & Boulanger, C. M. (2012). Flow cytometry: Retrospective, fundamentals and recent instrumentation. *Cytotechnology*, *64*(2), 109–130. https://doi.org/10.1007/s10616-011-9415-0

Postupna, N. O., Latimer, C. S., Keene, C. D., Montine, K. S., Montine, T. J., & Darvas, M. (2018). Flow cytometric evaluation of crude synaptosome preparation as a way to study synaptic alteration in neurodegenerative diseases. *Neuromethods*, *141*, 297–310. https://doi.org/10.1007/978-1-4939-8739-9_17

Purves, D., Augustine, G. J., Fitzpatrick, D., Katz, L. C., LaMantia, A.-S., McNamara, J. O., & Williams, S. M. (2001a). Chemical Synapses. In *Neuroscience. 2nd edition*. Sinauer Associates. https://www.ncbi.nlm.nih.gov/books/NBK11009/

Purves, D., Augustine, G. J., Fitzpatrick, D., Katz, L. C., LaMantia, A.-S., McNamara, J. O., & Williams, S. M. (2001b). Long-Term Synaptic Potentiation. In *Neuroscience. 2nd edition*. Sinauer Associates. https://www.ncbi.nlm.nih.gov/books/NBK10878/

Ramirez, A., & Arbuckle, M. R. (2016). Synaptic Plasticity: The Role of Learning and Unlearning in Addiction and Beyond. *Biological Psychiatry*, *80*(9), e73–e75. https://doi.org/10.1016/j.biopsych.2016.09.002

Richter, K. N., Wildhagen, H., Helm, M. S., Ußling, J.-E., Schikorski, T., & Rizzoli, S. O. (2018). Comparative synaptosome imaging: A semi-quantitative method to obtain copy numbers for synaptic and neuronal proteins. *Scientific Reports*, *8*, 14838. https://doi.org/10.1038/s41598-018-33130-6

Romito, J. W., Turner, E. R., Rosener, J. A., Coldiron, L., Udipi, A., Nohrn, L., Tausiani, J., & Romito, B. T. (2021). Baclofen therapeutics, toxicity, and withdrawal: A narrative review. *SAGE Open Medicine*, *9*, 20503121211022197. https://doi.org/10.1177/20503121211022197

Ross, A., & Willson, V. L. (2017). One-Sample T-Test. In A. Ross & V. L. Willson (Eds.), *Basic and Advanced Statistical Tests: Writing Results Sections and Creating Tables and Figures* (pp. 9–12). SensePublishers. https://doi.org/10.1007/978-94-6351-086-8_2

Rowe, R. K., Griffiths, D. R., & Lifshitz, J. (2016). Midline (Central) Fluid Percussion Model of Traumatic Brain Injury. *Methods in Molecular Biology (Clifton, N.J.)*, *1462*, 211–230. https://doi.org/10.1007/978-1-4939-3816-2_13

Sakai, J. (2020). How synaptic pruning shapes neural wiring during development and, possibly, in disease. *Proceedings of the National Academy of Sciences*, *117*(28), 16096–16099. https://doi.org/10.1073/pnas.2010281117

Sandoval, M. E., Horch, P., & Cotman, C. W. (1978). Evaluation of glutamate as a hippocampal neurotransmitter: Glutamate uptake and release from synaptosomes. *Brain Research*, *142*(2), 285–299. https://doi.org/10.1016/0006-8993(78)90636-4

Santos, E., & Noggle, C. A. (2011). Synaptic Pruning. In S. Goldstein & J. A. Naglieri (Eds.), *Encyclopedia of Child Behavior and Development* (pp. 1464–1465). Springer US. https://doi.org/10.1007/978-0-387-79061-9_2856

Scangos, K. W., State, M. W., Miller, A. H., Baker, J. T., & Williams, L. M. (2023). New and emerging approaches to treat psychiatric disorders. *Nature Medicine*, *29*(2), Article 2. https://doi.org/10.1038/s41591-022-02197-0

Schafer, D. P., Lehrman, E. K., Kautzman, A. G., Koyama, R., Mardinly, A. R., Yamasaki, R., Ransohoff, R. M., Greenberg, M. E., Barres, B. A., & Stevens, B. (2012). Microglia Sculpt Postnatal Neural Circuits in an Activity and Complement-Dependent Manner. *Neuron*, *74*(4), 691–705. https://doi.org/10.1016/j.neuron.2012.03.026

Schrimpf, S. P., Meskenaite, V., Brunner, E., Rutishauser, D., Walther, P., Eng, J., Aebersold, R., & Sonderegger, P. (2005). Proteomic analysis of synaptosomes using isotope-coded affinity tags and mass spectrometry. *PROTEOMICS*, *5*(10), 2531–2541. https://doi.org/10.1002/pmic.200401198

Sellgren, C. M., Gracias, J., Watmuff, B., Biag, J. D., Thanos, J. M., Whittredge, P. B., Fu, T., Worringer, K., Brown, H. E., Wang, J., Kaykas, A., Karmacharya, R., Goold, C. P., Sheridan, S. D., & Perlis, R. H. (2019). Increased synapse elimination by microglia in schizophrenia patient-derived models of synaptic pruning. *Nature Neuroscience*, *22*(3), 374–385. https://doi.org/10.1038/s41593-018-0334-7

Simerly, R. B. (2002). Wired for reproduction: Organization and development of sexually dimorphic circuits in the mammalian forebrain. *Annual Review of Neuroscience*, *25*, 507–536. https://doi.org/10.1146/annurev.neuro.25.112701.142745

Singh, I. N., Sullivan, P. G., Deng, Y., Mbye, L. H., & Hall, E. D. (2006). Time course of post-traumatic mitochondrial oxidative damage and dysfunction in a mouse model of focal traumatic brain injury: Implications for neuroprotective therapy. *Journal of Cerebral Blood Flow and Metabolism: Official Journal of the International Society of Cerebral Blood Flow and Metabolism*, *26*(11), 1407–1418. https://doi.org/10.1038/sj.jcbfm.9600297

Singh, J. B., Fedgchin, M., Daly, E. J., De Boer, P., Cooper, K., Lim, P., Pinter, C., Murrough, J. W., Sanacora, G., Shelton, R. C., Kurian, B., Winokur, A., Fava, M., Manji, H., Drevets, W. C., & Van Nueten, L. (2016). A Double-Blind, Randomized, Placebo-Controlled, Dose-Frequency Study of Intravenous Ketamine in Patients With Treatment-Resistant Depression. *The American Journal of Psychiatry*, *173*(8), 816–826. https://doi.org/10.1176/appi.ajp.2016.16010037

Soghomonian, J. J., Sethares, C., & Peters, A. (2010). Effects of age on axon terminals forming axosomatic and axodendritic inhibitory synapses in prefrontal cortex. *Neuroscience*, *168*(1), 74–81. https://doi.org/10.1016/j.neuroscience.2010.03.020

Sokolow, S., Henkins, K. M., Bilousova, T., Miller, C. A., Vinters, H. V., Poon, W., Cole, G. M., & Gylys, K. H. (2012). AD synapses contain abundant Aβ monomer and multiple soluble oligomers, including a 56 kDa assembly. *Neurobiology of Aging*, *33*(8), 1545–1555. https://doi.org/10.1016/j.neurobiolaging.2011.05.011

Sokolow, S., Luu, S. H., Headley, A. J., Hanson, A. Y., Kim, T., Miller, C. A., Vinters, H. V., & Gylys, K. H. (2011). High levels of synaptosomal Na+-Ca2+ exchangers (NCX1, NCX2, NCX3) co-localized with amyloid-beta in human cerebral cortex affected by Alzheimer's disease. *Cell Calcium*, *49*(4), 208–216. https://doi.org/10.1016/j.ceca.2010.12.008

Steinkamp, J. A., Romero, A., Horan, P. K., & Crissman, H. A. (1974). Multiparameter analysis and sorting of mammalian cells. *Experimental Cell Research*, *84*(1), 15–23. https://doi.org/10.1016/0014-4827(74)90374-7

Stephan, A. H., Barres, B. A., & Stevens, B. (2012). The Complement System: An Unexpected Role in Synaptic Pruning During Development and Disease. *Annual Review of Neuroscience*, *35*(1), 369–389. https://doi.org/10.1146/annurev-neuro-061010-113810

Stoliker, D., Egan, G. F., Friston, K. J., & Razi, A. (2022). Neural Mechanisms and Psychology of Psychedelic Ego Dissolution. *Pharmacological Reviews*, *74*(4), 876–917. https://doi.org/10.1124/pharmrev.121.000508

Südhof, T. (2013). Neurotransmitter Release: The Last Millisecond in the Life of a Synaptic Vesicle: Neuron. *Perspective*, *80*(3). https://doi.org/10.1016/j.neuron.2013.10.022

Tagge, C. A., Fisher, A. M., Minaeva, O. V., Gaudreau-Balderrama, A., Moncaster, J. A., Zhang, X.-L., Wojnarowicz, M. W., Casey, N., Lu, H., Kokiko-Cochran, O. N., Saman, S., Ericsson, M., Onos, K. D., Veksler, R., Senatorov, V. V., Kondo, A., Zhou, X. Z., Miry, O., Vose, L. R., … Goldstein, L. E. (2018). Concussion, microvascular injury, and early tauopathy in young athletes after impact head injury and an impact concussion mouse model. *Brain*, *141*(2), 422–458. https://doi.org/10.1093/brain/awx350

Tenreiro, P., Rebelo, S., Martins, F., Santos, M., Coelho, E. D., Almeida, M., Alves de Matos, A. P., & da Cruz E Silva, O. a. B. (2017). Comparison of simple sucrose and percoll based methodologies for synaptosome enrichment. *Analytical Biochemistry*, *517*, 1–8. https://doi.org/10.1016/j.ab.2016.10.015

Terletskaya, Ya. T., Himmelreich, N. H., & Sokolov, Yu. V. (1992). [20] - Presynaptic Activity of α-Latrotoxin: Purification and Properties. In P. M. Conn (Ed.), *Methods in Neurosciences* (Vol. 8, pp. 283–297). Academic Press. https://doi.org/10.1016/B978-0-12-185266-5.50025-7

Thiel, G. (1993). Synapsin I, Synapsin II, and Synaptophysin: Marker Proteins of Synaptic Vesicles. *Brain Pathology*, *3*(1), 87–95. https://doi.org/10.1111/j.1750-3639.1993.tb00729.x

Trebesova, H., & Grilli, M. (2023). Synaptosomes: A Functional Tool for Studying Neuroinflammation. *Encyclopedia*, *3*(2), Article 2. https://doi.org/10.3390/encyclopedia3020027

van Amerongen, S., Caton, D. K., Pijnenburg, Y. A. L., Scheltens, P., & Vijverberg, E. G. B. (2022). Clinical Features of Patients with Alzheimer's Disease and a History of Traumatic Brain Injury. *Dementia and Geriatric Cognitive Disorders Extra*, *12*(3), 122–130. https://doi.org/10.1159/000526243

Vargas, M. V., Meyer, R., Avanes, A. A., Rus, M., & Olson, D. E. (2021). Psychedelics and Other Psychoplastogens for Treating Mental Illness. *Frontiers in Psychiatry*, *12*, 727117. https://doi.org/10.3389/fpsyt.2021.727117

Visser, E., & Schug, S. A. (2006). The role of ketamine in pain management. *Biomedicine & Pharmacotherapy*, *60*(7), 341–348. https://doi.org/10.1016/j.biopha.2006.06.021

Wadhwa, R. R., & Marappa-Ganeshan, R. (2023). T Test. In *StatPearls*. StatPearls Publishing. http://www.ncbi.nlm.nih.gov/books/NBK553048/

Weiler, I. J. (2009). Synaptosomes—ScienceDirect. In *Encyclopedia of Neuroscience* (pp. 815–818). Academic Press. https://www.sciencedirect.com/science/article/abs/pii/B9780080450469020453?via%3Dihub

Wells, G. B., Lopez, M. C., & Tanaka, J. C. (1999). The effects of ibogaine on dopamine and serotonin transport in rat brain synaptosomes. *Brain Research Bulletin*, *48*(6), 641–647. https://doi.org/10.1016/S0361-9230(99)00053-2

Whittaker, V. P. (1959). The isolation and characterization of acetylcholine-containing particles from brain. *Biochemical Journal*, *72*(4), 694–706.

Whittaker, V. P. (1993). Thirty years of synaptosome research. *Journal of Neurocytology*, *22*(9), 735–742. https://doi.org/10.1007/BF01181319

Wiesel, T. N., & Hubel, D. H. (1963). Single-cell responses in striate cortex of kittens deprived of vision in one eye. *Journal of Neurophysiology*, *26*(6), 1003–1017. https://doi.org/10.1152/jn.1963.26.6.1003

Willer, B. S., Haider, M. N., Bezherano, I., Wilber, C. G., Mannix, R., Kozlowski, K., & Leddy, J. J. (2019). Comparison of Rest to Aerobic Exercise and Placebo-like Treatment of Acute Sport-Related Concussion in Male and Female Adolescents. *Archives of Physical Medicine and Rehabilitation*, *100*(12), 2267–2275. https://doi.org/10.1016/j.apmr.2019.07.003

Willing, J., & Juraska, J. M. (2015). The Timing of Neuronal Loss Across Adolescence in the Medial Prefrontal Cortex of Male and Female Rats. *Neuroscience*, *301*, 268–275. https://doi.org/10.1016/j.neuroscience.2015.05.073

Wu, Q., Sun, M., Bernard, L. P., & Zhang, H. (2017). Postsynaptic density 95 (PSD-95) serine 561 phosphorylation regulates a conformational switch and bidirectional dendritic spine structural plasticity. *The Journal of Biological Chemistry*, *292*(39), 16150–16160. https://doi.org/10.1074/jbc.M117.782490

Xie, C., Xiang, S., Shen, C., Peng, X., Kang, J., Li, Y., Cheng, W., He, S., Bobou, M., Broulidakis, M. J., van Noort, B. M., Zhang, Z., Robinson, L., Vaidya, N., Winterer, J., Zhang, Y., King, S., Banaschewski, T., Barker, G. J., … Feng, J. (2023). A shared neural basis underlying psychiatric comorbidity. *Nature Medicine*, *29*(5), Article 5. https://doi.org/10.1038/s41591-023-02317-4

Xu, Y., McArthur, D. L., Alger, J. R., Etchepare, M., Hovda, D. A., Glenn, T. C., Huang, S., Dinov, I., & Vespa, P. M. (2010). Early nonischemic oxidative metabolic dysfunction leads to chronic brain atrophy in traumatic brain injury. *Journal of Cerebral Blood Flow and Metabolism: Official Journal of the International Society*

of Cerebral Blood Flow and Metabolism, *30*(4), 883–894. https://doi.org/10.1038/jcbfm.2009.263

Yang, C., Hu, Y.-M., Zhou, Z.-Q., Zhang, G.-F., & Yang, J.-J. (2013). Acute administration of ketamine in rats increases hippocampal BDNF and mTOR levels during forced swimming test. *Upsala Journal of Medical Sciences*, *118*(1), 3–8. https://doi.org/10.3109/03009734.2012.724118

Yu, H., Majewska, A. K., & Sur, M. (2011). Rapid experience-dependent plasticity of synapse function and structure in ferret visual cortex in vivo. *Proceedings of the National Academy of Sciences of the United States of America*, *108*(52), 21235–21240. https://doi.org/10.1073/pnas.1108270109

Zaqout, S., & Kaindl, A. M. (2016). Golgi-Cox Staining Step by Step. *Frontiers in Neuroanatomy*, *10*, 38. https://doi.org/10.3389/fnana.2016.00038

Zimmermann, H. (2018). Victor P. Whittaker: The Discovery of the Synaptosome and Its Implications. In *Synaptosomes* (pp. 2–26). Humana Press. https://experiments.springernature.com/articles/10.1007/978-1-4939-8739-9_2

Zweckberger, K., Erös, C., Zimmermann, R., Kim, S.-W., Engel, D., & Plesnila, N. (2006). Effect of early and delayed decompressive craniectomy on secondary brain damage after controlled cortical impact in mice. *Journal of Neurotrauma*, *23*(7), 1083–1093. https://doi.org/10.1089/neu.2006.23.1083

APPENDIX A

SYNAPTIC FLOW PROTOCOL (ADAPTED FROM KRUKOWSKI ET AL., 2021)

Required Materials:

- HEPES (Cytiva HyClone, SH 30237.01, Logan, Utah)
- 1X Phosphate-buffered saline (PBS)
- 2% Paraformaldehyde (PFA) (Fisher Scientific, 50-276-34) in PBS
- Cytofix/Cytoperm solution (BD Biosciences, 554655)
- 0.32 M Sucrose
- Perm Wash (BD Biosciences, 554723)
- Primary Antibodies: Rb anti-Synapsin 1 (presynaptic marker; Millipore, MAB1543), Ms anti-PSD95 (postsynaptic marker; Thermofisher, MA1-046)
- Secondary Antibodies: Anti-mouse Alexa Fluor 488 (Invitrogen, A-11001), APC (Allophycocyanin) goat anti-rabbit (Invitrogen, A10931)
- Teflon/Glass homogenizer (DWK Life Sciences (Kimble) Dounce Tissue Grinder, 885303-0002)
- Tubes with labels stored in 4°C or -20°C (different colored tops for different antibodies)
    - 15 mL tubes
    - 1.5 mL tubes
    - FACS tubes
    - 50 mL conical vial for samples (triplicate)
    - 50 mL tubes for unstained (single)

Making Buffers:

HEPES/0.32 M Sucrose (fresh)

1. Add 500 µL HEPES (Sigma-Aldrich, H0887) to 49.5 mL dH_2O in 50 mL tube then vortex to mix well.
2. Add 25 mL of HEPES/water solution made in Step 1 to a clean 50 mL tube and add 2.73 g sucrose, vortex to mix well while protected from light with foil.

*For 10 mL of HEPES buffer, add 1.097 g of sucrose to 9.9 mL of dH_2O and 0.1 mL of HEPES

Perm/Wash (BD Biosciences, 554723) - wash and permeabilize cells for antibody staining

1. To prepare perm wash working solution (1X), add 5 mL perm wash stock solution (10X) in 45 mL of dH_2O

Cytofix/Cytoperm (0.1X) (BD Biosciences, 554655)

1. Add 1 mL of Cytofix/Cytoperm solution (1X) to 9 mL dH_2O

2% PFA in PBS

1. To make 2% PFA working solution, add 2 mL of 4% PFA to 98 mL PBS.

BEFORE STARTING PROTOCOL:

1. Obtain cooler and bucket of ice that can be replenished throughout the day.
2. Place Dounce glass homogenization tubes on ice
3. Cool centrifuges (Beckman Coulter Allegra X-15R Centrifuge and Eppendorf 5425 R) to 4°C

4. Place 1.5 mL tubes to cool in -20°C.

PROTOCOL:

I. SYNAPTOSOME ISOLATION

1. Add 1 mL HEPES/sucrose to the homogenization tube.
2. Using spatula, place the sample into the homogenization tube ensuring that it is submerged. Place the tissue tube back on ice.
3. Homogenize 10 strokes (1 stroke = 1 full up and down motion with a full clockwise twist of the homogenizer)
4. Pipette the lysate into a clean 15 mL tube (use smaller pipette to reach into homogenization tube)
5. Rinse the tissue tube and homogenization tube using 1 mL HEPES/sucrose each then add the lysates to the 15 mL tube.
6. Rinse the homogenization tube using 1 mL HEPES/sucrose once more and add to 15 mL tube (total volume in the 15 mL tube: 3 mL + sample)
7. Spin the 15 ml tubes using Beckman Coulter Allegra X-15R Centrifuge at 1,200 RCF @ 4°C for 10 min.
8. Check the 15 mL tubes for pellets before continuing.
9. Add ~1-1.5 mL of supernatant to 2 x 1.5 mL tubes.
    - Synaptosomes are in supernatant, keep pellets on ice in case needed further.
10. Spin the 1.5 mL tubes at 13,000 RCF @ 4°C for 20 min using Eppendorf 5425 R (adjust temp to 2°C if sample is warmed)

11. Check the 1.5 mL tubes for pellets before continuing.

12. Resuspend the pellet in 200 µl of PBS (~20 up/downs with pipette with new tip for each sample and standardize the number of times across all samples)

13. Combine the duplicate of samples into one 1.5 mL tube and vortex gently to mix well before performing BCA.

14. Run normal BCA with these re-suspended samples - triplicate.

II. BCA ASSAY

1. Sample Preparation:
    1. Add 5 µL of sample to 120 µL water in a tube to make a 25x dilution (make 50x dilution by adding 5 µL of sample to 245 µL water if using rat brains)
2. Standard Preparation:
    1. Add dH_2O and BSA to Eppendorf tube until homogenous.
3. The first three columns of the plate are for the Standard Curve

Protein Concentration (µg/µL)	BSA (µL)	dH_2O (µL)
0	0	100
1.5	3	97
3	6	94

4.5	9	91
6	12	88
7.5	15	85
9	18	82
10.5	21	79

4. To each well of the triplicate, add 25 µL of diluted sample or standard.
5. Calculate developer (200 µL per well)
    1. 8 standards + _____ samples + 2 extras = _____ x 3 = _____ wells
    2. _____ wells x 200 µL/well = _____µL reagent A
    3. _____ reagent A / 50 = _____µL reagent B
6. Make developer.
    1. Add Reagent A and Reagent B to a 50 mL conical vial wrapped in foil (light sensitive)
7. Add 200 µL of developer to each well.
8. Incubate for 37 ℃ for 30 minutes at 300 RPMS.
9. Cool plate to room temperature (~5 minutes).
10. Read plate and put plate values into Protein Calculation Excel sheet.

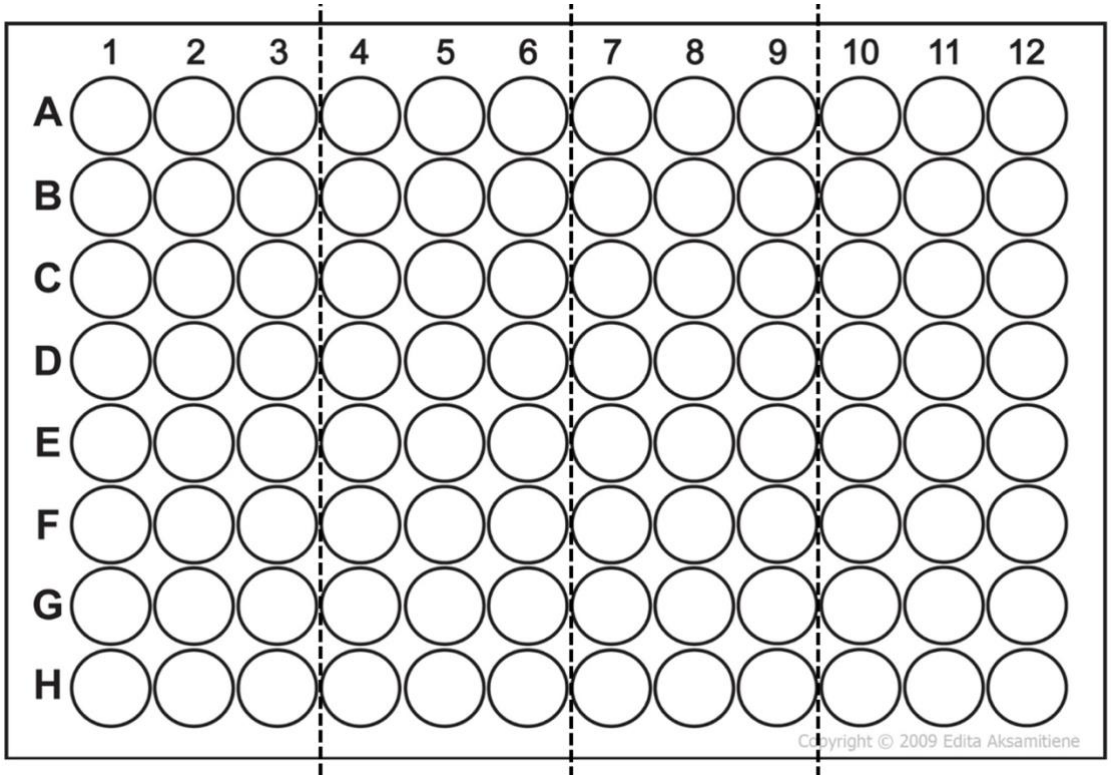

11. Using the linear graph given by the standards, find the concentration of protein in the sample.

12. Undo the dilution of the sample to find the actual protein concentration to determine the amount of antibody needed.

    1. Final protein concentration should be 75 µg/mL.

III. ANTIBODY STAINING

1. Using data from the Protein Calculation Excel sheet, add appropriate PBS volume to clean 5 mL tubes. The number of tubes needed is calculated by having 2-3 replicates per sample and a negative control.
2. Obtain clean, labeled 1.5 mL tubes stored at -20 ℃

3. Add 200 µL of sample to each respective tube with new tip for each sample and vortex to mix well.
4. Add 100 µL of Cytofix/Cytoperm to each sample tube, vortex to mix well and place on ice for 20 min.
5. Wash samples using 750 µL of perm wash working solution.
6. Pipette to mix, then vortex to mix well.
7. Centrifuge at 13,000 RCF for 5 minutes at 4 ℃ using Eppendorf 5425 R
    1. Check for a pellet in the tubes, only continue if a pellet is present.
8. Dump supernatant and repeat wash through spin (Steps 5 to 8)
9. Add blocking agent (0.2 µL Fc Block) and incubate for 10-12 minutes in the dark at 4 °C.
    1. Wash not needed.
10. Make the primary and secondary antibodies by adding antibodies to PBS, calculated using the designed Antibody Calculation Excel sheet, and place on ice.
11. Dump the supernatant without disrupting the pellet.
12. Add a drop of UltraComp EBeads to 3 tubes to make beads that are unstained, stained with presynaptic and postsynaptic beads, respectively.
13. Add 400 µL of respective primary antibodies, vortex to mix well, and incubate for 30 min at room temperature.
    1. Vortex halfway through incubation to ensure proteins get the opportunity to attach to antibodies.
14. Repeat wash, mix, spin, dump (Steps 5 to 8)
    1. For beads - leave 50 µL at the bottom during washes

15. Dump the supernatant without disrupting pellet.

16. Add 400 µL of the secondary antibodies and incubate for 30 min at 4 °C.

    1. Vortex halfway through incubation to ensure proteins get the opportunity to attach to antibodies.

17. Repeat wash, mix, spin, dump (Steps 5 to 8) for a total of three times for each tube.

18. Remove the remaining supernatant.

19. Add 200 µL of 2% PFA to the pellets, pipet, and vortex to mix well before transferring to FACS tube and storing at 4 °C.

Notes: Flow cytometry gating is based on 1, 3, 6 µm beads

APPENDIX B

FLOW-ASSISTED CELL SORTING (FACS) BUFFER PROTOCOL (1 L)

Materials:

1. HBSS without Ca or Mg (1 L)
2. BSA (0.5 g)
3. 2 mM EDTA (4 mL 1.5 M EDTA)
4. 25 mM HEPES (25 mL 1M HEPES)
5. Sodium azide (NaN_3) (0.9 g)

Protocol:

1. Stir to mix well.

98

APPENDIX C

FLOW CYTOMETER USER GUIDE (NOVOCYTE QUANTEON)

Preparing Controls:

1. To set up compensation controls in tubes,
    a. 1 drop of Ultracomp EBeads added to 1 µL of secondary antibody and 300 µL of FACS buffer.
    b. Set up a negative control (beads only)

Preparing Samples for Flow:

1. Add 200 µL of FACS buffer to samples.
    a. Can try out different dilutions if needed.

Machine: Agilent NovoCyte Quanteon Flow Cytometer

1. Turn on the machine ~10 minutes before intended use, check if fluids are at at appropriate levels.
2. Complete Quality Control (QC) if not yet completed for the day.
    a. If QC needed, tube of QC particles is in dairy case to the left of flow machine.
    b. If fresh beads needed, mix 1 drop of beads with 500 µL of PBS or 400 µL of PBS and 100 µL of 1X NovoRinse.
    c. Vortex the diluted beads to mix well and insert the tube onto the tube holder.
    d. Click QC Test: 'Instrument > Operation > QC Test'
    e. Enter QC Particles Lot ID (Our last Lot ID was SS000895)
    f. Click 'Next > Run', then Report when QC is finished.

g. Ensure all the results say ‘Pass’, then click ‘Finish’. If results do not say ‘Pass’ (eg: ‘Acceptable/Fail’, repeat QC Test on fresh beads and call technical support if issue persists.

3. Create an experiment by right clicking under ‘Experiment Manager.’
    a. An untitled experiment will automatically generate in the right-hand side of the NovoExpress software (Experiment Manager) but you can also import a previously saved template
4. Create compensation controls using ‘Auto Compensation’.
    a. Add your parameters and compensation controls by right clicking on untitled.ncf and selecting ‘New Auto Compensation’.
        i. Here, you can choose how to you would like to run compensation (height vs area, median vs means etc)
        ii. Select and rename your chosen parameters.
        iii. Clicking ‘Unstained’ means that you are providing a universal unstained sample for all single-stained controls. If you do not have a universal unstained control, ensure that each single stained sample has a positive and negative population within the sample and unclick ‘Unstained’.
5. Run compensation tubes by placing corresponding tube on the holder and clicking ‘Run.’
6. After collecting 10,000 events, the FSC vs SSC and positive/negative gates would be automatically adjusted. To change these, click on the gate you would like to alter and delete it using the keyboard or adjust it using arrows.

a. Repeat this with all single-stained compensation controls.
b. When done, a compensation matrix will automatically generate (double click to view) and the font of the Compensation will turn blue in Experiment Manager
c. Apply the compensation matrix to the experiment by clicking and dragging Compensation to the untitled.ncf and selecting ‘New Specimen’ or make a new Specimen and Sample by right clicking and selecting ‘Rename’.

7. Select the parameters for running your sample (left of page, under ‘Cytometer Setting’)
    a. Under ‘Stop Condition’, select the condition under which you would like for data collection to stop: # of events, (select which gate you want or ‘ungated’ would be the default), time, or volume of sample.
        i. Note: If volume is selected, account for extra to be removed from sample (eg: if the stop condition is 100 µL, the sample should at least be resuspended in 150 µL)
        ii. Only 20-30 µL needed for samples to generate 30,000 events due to them having a higher concentration than flow beads.
8. Under ‘Flow Rate’, select the speed that your sample would be collected at using the slider for finer adjustments.
    a. 10 µL/min for samples

b. Under ‘Threshold’, select the threshold of events you would like to exclude from collection - default is 100,000 on FSC-H (recommended for most cells)

c. At the bottom left of NovoExpress, the following options can also be selected:

    i. Absolute counting: the settings can be adjusted under ‘Sample > Absolute Count Setting’ before or after acquisition.

    ii. Rinse after sample: this reduces carry over between samples.

    iii. Recover remaining samples: After samples are acquired, leave the tubes in the holder and the machine will return any unused samples.

d. To apply these conditions to all samples, in the Experiment Manager under the sample that is being adjusted, drag, and drop the Cytometer Setting to the Specimen you’d like to apply it to.

9. Creating Gates

    a. Dot plots, contour plots, density plots and histograms can be made by clicking their icons at the top of the screen.

    b. The x- and y-axes can be adjusted by clicking on the name and selecting the desired parameter.

    c. The scale can be adjusted by right clicking on the axis and clicking ‘Setting.’

    d. Create square, oval, polygon, and freehand gates by clicking on the icon, located in the same bar as the plots.

e. To apply just the cells selected in one gate to another plot, right click a new plot and select ‘Gating > Choose Gate’.

10. When completed, the files can be saved as ‘.ncf ‘(default for NovoExpress analysis) or exported to ‘.fcs’
11. Turn the machine off by pressing the Power button on the side of the machine. It would not be necessary to run bleach or tubes of water.

APPENDIX D

PROTEIN CALCULATION SHEET USED TO STANDARDIZE SAMPLE PROTEIN CONCENTRATION

BSA ug (X)	OD (Y)
0	
1.5	
3	
4.5	
6	
7.5	
9	
10.5	

r^2	
slope2	
intercept2	

Protein Assay	
Sample Volume (ul):	25
Dillution Factor 1:	50

Synaptic Flow	
Volume per Sample (ul):	200
Final Protein Conc. (ug/ml):	75

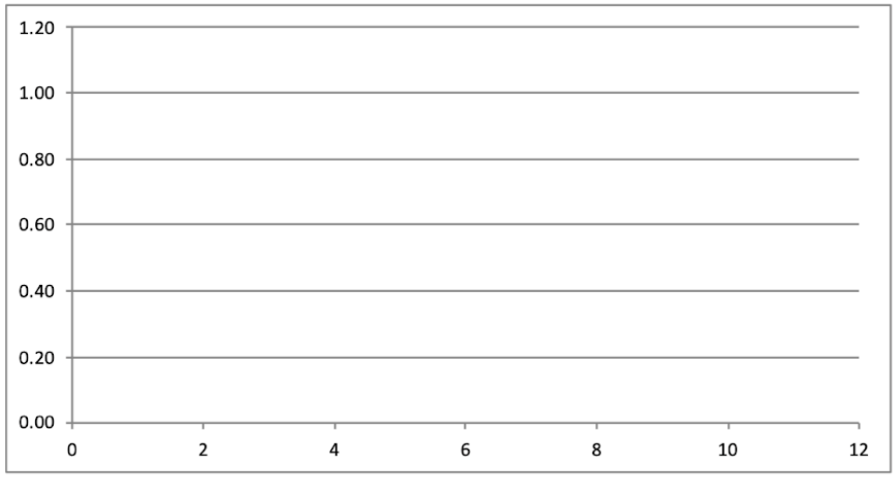

						Sample Info		
	Sample Name	OD for Protein	Total Protein per Well	Protein Concentration	Number of Tubes	Sample Volume	1X PBS Volume	Total Volume
#			(ug)	(ug/ul)	(#)	(ul)	(ul)	(ul)
1								
2								
3								
4								

APPENDIX E

ANTIBODY CALCULATION SHEET USED TO CALCULATE ANTIBODY DILUTIONS

Antibody	Catalog #	Link to Data Sheet	Stock Concentration (ug/uL)	Labelling Ratio for Synaptosomes (ug:uL)	Ratio in decimals	Tubes needed	Volume of diluted antibody added to each tube (µL)	Total Volume (µL)	PBS to add (µL)	Antibody to add (µL)	Total Antibody Needed (µL)
Rb anti-Synapsin 1	Millipore, MAB1543	https://www.emdmillipore.	1	1 : 200	0.005		400		0	0	0
Ms anti-PSD95 Monoclonal antibody	Thermofisher, MA1-046	https://www.thermofisher.	1	1 : 200	0.005		400		0	0	0
488 anti-mouse	Invitrogen, A-11001	https://www.thermofisher.	0.5	1 : 100	0.01		400		0	0	0
APC (Allophycocyanin) goat anti-rabbit	Invitrogen, A10931	https://www.thermofisher.	1	1 : 400	0.0025		400		0	0	0

APPENDIX F

IACUC ANIMAL USE APPROVAL

THE UNIVERSITY OF ARIZONA
Research
Innovation & Impact

Administration 601
PO Box 210066
Tucson, AZ 85721-0066
Ofc: 520-621-3513
Fax: 520-621-7507

Verification of Institutional Animal Care and Use Committee (IACUC)

Review and Approval

This protocol has been reviewed by the IACUC and the work may commence at this time. This approval only authorizes the activities reviewed by the IACUC as described on the final version of the protocol.

Principal Investigator: Lifshitz, Jonathan
Department: Child Health - PBC

Protocol Number: 13-460
Title: Translational neurotrauma research [+DoD] [+MOU] [+VA]

Approval Date: 08/28/2019
Expiration Date: 08/28/2022

Funding Sources: Departmental
DoD: AZ160056
VA: RX002472-01
VA: 36C25819D0025
NIH/NINDS 1R21NS120022-01
Arizona Alzheimer's Consortium
Arizona Biomedical Research Commission
Diane and Bruce Halle Foundation
American Sleep Society

Grant to Protocol Review: Not Applicable

Additional Notes Concerning Submission: Addition of tactile allodynia sensory task.

The Principal Investigator (PI) is responsible for all work conducted on this protocol. As such, the PI must ensure that:

- The protocol will be conducted in accordance with all applicable federal and institutional policies, procedures and regulations, including the PHS Policy on Humane Care and Use of Laboratory Animals, USDA regulations (9 CFR Parts 1, 2, 3), the Federal Animal Welfare Act (7 USC 2131 et. Seq.), the Guide for the Care and Use of Laboratory Animals, and all relevant institutional regulations and policies regarding animal care and use at the University of Arizona.
- All procedures involving animals will be carried out humanely and as described in the approved protocol.
- IACUC approval will be secured before initiating any change in the study design or procedures listed on this protocol. Protocol participants understand that all amendments must be approved by the IACUC prior to implementation.
- Work performed without IACUC approval is not published with certification of IACUC approval.
- All individuals working autonomously on this protocol are qualified to conduct procedures involving animals, are competent in the techniques cited in the protocol, and will maintain appropriate and complete animal records. All untrained staff will be sufficiently supervised until competency is achieved.
- The IACUC is notified regarding any unanticipated deaths or unexpected study results or a phenotype that negatively impacts the welfare of the animals, including but not limited to those that require veterinary care or treatment not described in the approved protocol.
- The hazards listed on this protocol will be handled as per Research Laboratory Safety Services (RLSS) guidelines and stipulations. Work with hazards is not performed until RLSS approval has been granted.

John P. Konhilas, PhD
IACUC Chair